JOURNAL OF PETROLOGY | VOLUME 44 | NUMBER 2 | PAGES 305–327 | 2003

Anticlockwise *P–T* Path of Granulites from the Monte Castelo Gabbro (Órdenes Complex, NW Spain)

JACOBO ABATI[1]*, RICARDO ARENAS[1], JOSÉ RAMÓN MARTÍNEZ CATALÁN[2] AND FLORENTINO DÍAZ GARCÍA[3]

[1]DEPARTAMENTO DE PETROLOGÍA Y GEOQUÍMICA, FACULTAD DE C.C. GEOLÓGICAS, UNIVERSIDAD COMPLUTENSE, 28040 MADRID, SPAIN

[2]DEPARTAMENTO DE GEOLOGÍA, UNIVERSIDAD DE SALAMANCA, 37008 SALAMANCA, SPAIN

[3]DEPARTAMENTO DE GEOLOGÍA, UNIVERSIDAD DE OVIEDO, 33005 OVIEDO, SPAIN

RECEIVED JULY 1, 2001; REVISED TYPESCRIPT ACCEPTED AUGUST 13, 2002

The study of mafic and aluminous granulites from the Monte Castelo Gabbro (Órdenes Complex, NW Spain) reveals an anticlockwise P–T *path that we interpret as related to the tectonothermal activity in a magmatic arc, probably an island arc. The* P–T *path was obtained after a detailed study of the textural relationships and mineral assemblage succession in the aluminous granulites, and comparing these with an appropriate petrogenetic grid. Additional thermobarometry was also performed. The granulites are highly heterogeneous, with distinct compositional domains that may alternate even at thin-section scale. Garnets are generally idiomorphic to subidiomorphic, and in certain domains of the aluminous granulites they show overgrowths forming xenomorphic coronas around a more or less idiomorphic core. Both types of garnets show significant Ca enrichment at the crystal rims, which, together with the other mineralogical and textural characteristics, is compatible with a pressure increase with low* T *variation.* P–T *estimations indicate a peak of* T *>800°C and* P *~ 9·5 kbar, attained after a significant increase in pressure that took place at high temperatures (in the sillimanite field). We suggest that this kind of trajectory, probably anticlockwise, is compatible only with a terrane heated by an intense magmatic activity after or during tectonic crustal thickening (magmatic injection at the base and/or into the crust), which is characteristic of magmatic arcs.*

KEY WORDS: *granulites; garnet zoning; anticlockwise* P–T *path; Iberian Massif; NW Spain*

INTRODUCTION

Thermobarometric estimations in high-*T* metamorphic rocks are subject to important uncertainties, because the chemical composition of metamorphic peak minerals is frequently modified by retrograde diffusion phenomena, especially with respect to Fe–Mg exchanges (Spear & Florence, 1992; Carlson & Schwarze, 1997). Hence, in many cases, an adequate textural interpretation and deduction of the reaction sequence, in combination with the use of an appropriate petrogenetic grid, is a more reliable way to constrain the *P–T* path. Moreover, this approach facilitates the selection of relevant mineral assemblages and compositions for thermobarometry, and the comparison of the obtained quantitative *P–T* values with the petrogenetic grid makes it possible to check their mutual compatibility.

This approach has been followed in this investigation, devoted to the study of mafic and aluminous granulites from the Monte Castelo Gabbro, located in the uppermost unit of the Órdenes Complex (NW Spain). The aluminous granulites show a complex textural evolution, which can be followed in terms of the temporal succession of mineral associations. The textures are rich and varied, which permits the reconstruction of equilibrium mineral assemblages for distinct periods during metamorphic evolution and, in some cases, allows us to distinguish which reactions are implicated in the progress from one assemblage to the next. The coexistence of the different

*Corresponding author. Telephone: 34-91-3945013. Fax: 34-91-5442535. E-mail: abati@geo.ucm.es

mineral assemblages in the aluminous granulites is possible mainly because of their strong heterogeneity, with distinct textural and compositional domains that may coexist in the same thin section. The mafic granulites do not exhibit such textural variation, but it is still possible to recognize parts of the metamorphic stages evidenced in the aluminous granulites.

Applying the petrogenic grid of Spear *et al.* (1999) to the aluminous granulites, we have constructed a fragment of the *P–T* path. In addition, we performed thermobarometry calculations using the mineral compositions of the appropriate assemblages and the TWQ method of Berman (1991). The results of the thermobarometry are slightly different from the results obtained using the petrogenetic grid. However, we believe that they are essentially compatible given the uncertainties in both the thermobarometry calculations and the assemblages in the petrogenetic grid. We conclude by interpreting the *P–T* path in a tectonic framework and by analysing its implications for the regional geology of the Órdenes Complex.

GEOLOGICAL SETTING

The Órdenes Complex is one of the allochthonous structures of the NW Iberian Massif (Fig. 1), whose emplacement in the axial part of the orogen took place during the Variscan continental collision. These structures consist of a stack of thrust sheets that are preserved in late, open synforms. Three main tectonostratigraphic ensembles have been identified in the Órdenes Complex, which are essentially the same as those recognized in the other allochthonous complexes of northwestern Iberia. These are, from bottom to top, the basal, ophiolitic and upper units. Assuming that the ophiolites represent a collisional suture, the underlying basal units are interpreted as belonging to the margin of Gondwana and the upper units are considered far-travelled terranes of yet unconstrained provenance (Arenas *et al.*, 1986; Martínez Catalán *et al.*, 1997, 1999). The general geological features and the evolution of the allochthonous complexes have been the subject of numerous studies [for a comprehensive review, see Martínez Catalán *et al.* (1999) and references therein].

The upper units of the Órdenes Complex can be subdivided into high-pressure and high-temperature (HP–HT) units, below, and intermediate-pressure (IP) units, structurally above, with the Monte Castelo Gabbro being one of the IP upper units. The upper units show the complexities typical of terranes that have been involved in more than one orogenic cycle. These rocks record a structural and metamorphic evolution related to an Early Ordovician orogenic event, which is locally overprinted by structures, fabrics and metamorphic features related to the Variscan orogenic cycle. The Early Ordovician event has been dated by U–Pb analyses of zircon, monazite, titanite and rutile at ~500–480 Ma (Abati *et al.*, 1999; Fernández Suárez *et al.*, 2002), and is probably responsible for the main metamorphism observed in both the HP–HT and the IP units. It can be inferred from the above studies that the HP metamorphism took place during the Early Ordovician cycle (Fernández-Suárez *et al.*, 2002), and the same age has been obtained for the IP metamorphism that formed the granulites of the units described in this paper (Abati *et al.*, 1999). Geochronological evidence for subsequent tectonothermal activity in these units is generally restricted to zones of intense Variscan reworking (essentially shear zones). Within these zones, monazite, titanite and rutile isotopic data indicate that a second metamorphic episode took place between ~400 and 380 Ma, i.e. during the Variscan cycle.

The IP upper units occupy most of the Órdenes Complex (Fig. 1). They include a very thick sequence of terrigenous metasediments, and large bodies of amphibolite, augengneiss and metagabbro. Metamorphic grade ranges from greenschist facies in the structurally uppermost part to IP granulite facies in the lower. The lowermost IP unit in the NW sector of the complex is a large, rounded metaigneous massif, the Monte Castelo Gabbro (MCG, Fig. 2). The MCG is tholeiitic in character (Andonaegui *et al.*, 2002), and has been dated at 499 ± 3 Ma (Abati *et al.*, 1999; U–Pb in zircons). The intrusion is composed of fine- to medium-grained two-pyroxene gabbro, with textures ranging from granular to intergranular and ophitic, and with an igneous mineral assemblage consisting of clinopyroxene, orthopyroxene, plagioclase, scarce olivine, biotite and hornblende. Ilmenite, titanite, and zircon are the main accessory minerals. The presence of olivine and the common ophitic textures point to a relatively shallow depth of emplacement.

Although most of the massif preserves its igneous texture and mineral assemblages, mafic granulites were formed in localized shear zones in the basal part of the MCG, whereas aluminous granulites developed during the high-temperature metamorphism of aluminous (probably metapelitic) enclaves inside the gabbro (Fig. 2). Monazites separated from the aluminous granulites yielded a U–Pb age of 496 Ma for the metamorphism (Abati *et al.*, 1999).

FIELD RELATIONSHIPS OF THE GRANULITES

The aluminous granulites are found as enclaves dispersed in the MCG. They appear as bodies of variable size that can reach >1 km in length and several hundreds of

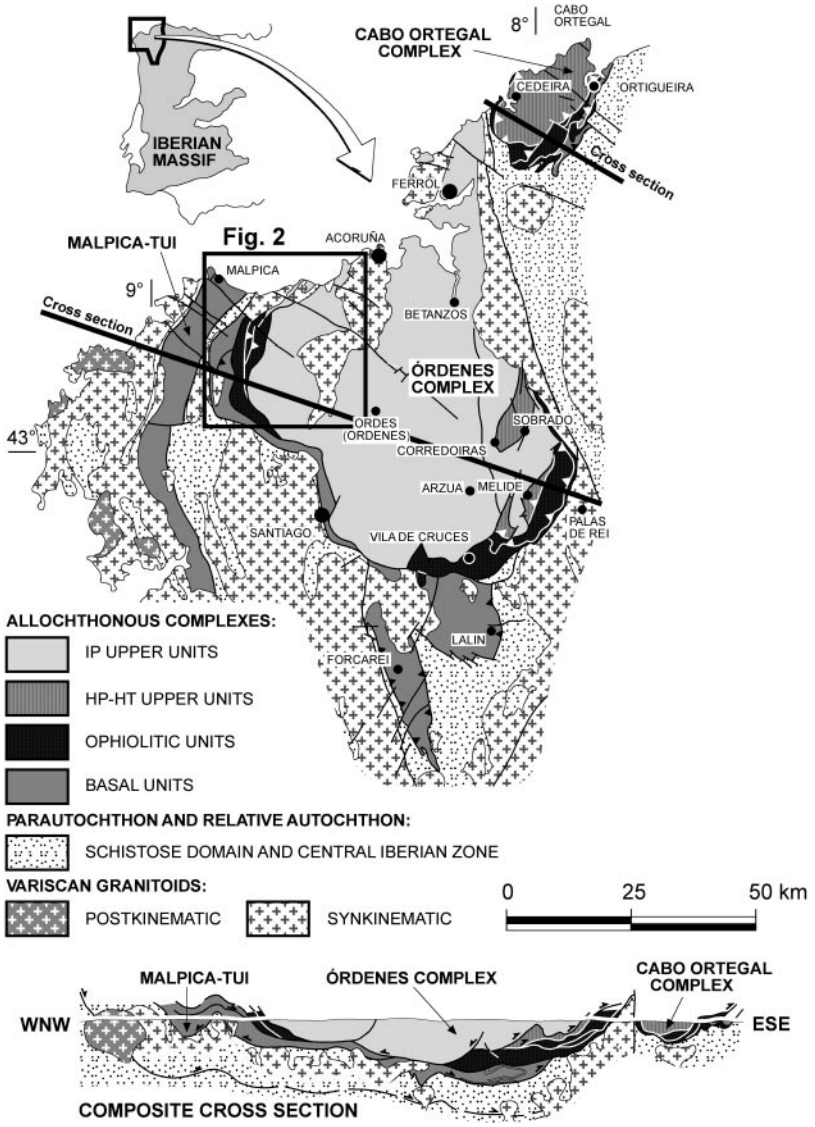

Fig. 1. Geological sketch and cross-section of the Órdenes Complex showing the various units.

metres in thickness, usually trending NW–SE (Fig. 2) and showing a high-T foliation with much evidence of partial melting, such as leucosomes oriented parallel to foliation (Fig. 3). The aluminous granulites are clearly heterogeneous at the outcrop scale, where lithological types with different textures and mineralogies can be recognized. Some granulitic types contain coarse garnets (up to 1 cm) surrounded by a granoblastic matrix formed by plagioclase, quartz, K-feldspar and subeuhedral elongated orthopyroxene.

In some outcrops of the central part of the gabbro massif, the enclaves are little deformed and show a medium- to coarse-grained granoblastic texture. Probably, this observation led previous workers (Warnaars, 1967) to interpret the metamorphism of the enclaves as the result of contact metamorphism, or of different contamination reactions between the gabbro and aluminium-rich materials. However, the evident high-T foliation excludes this possibility. Theoretically, another possible explanation of the relationships between the gabbro and its enclaves is that the latter represent lower-crustal xenoliths incorporated during magma ascent. However, this does not seem very likely, because the metamorphic conditions suggested by the mineral assemblages are comparable with those of the mafic granulites developed in shear zones crosscutting the basal part of the MCG (and are also compatible with the garnet zoning and the quantitative P–T estimations; see

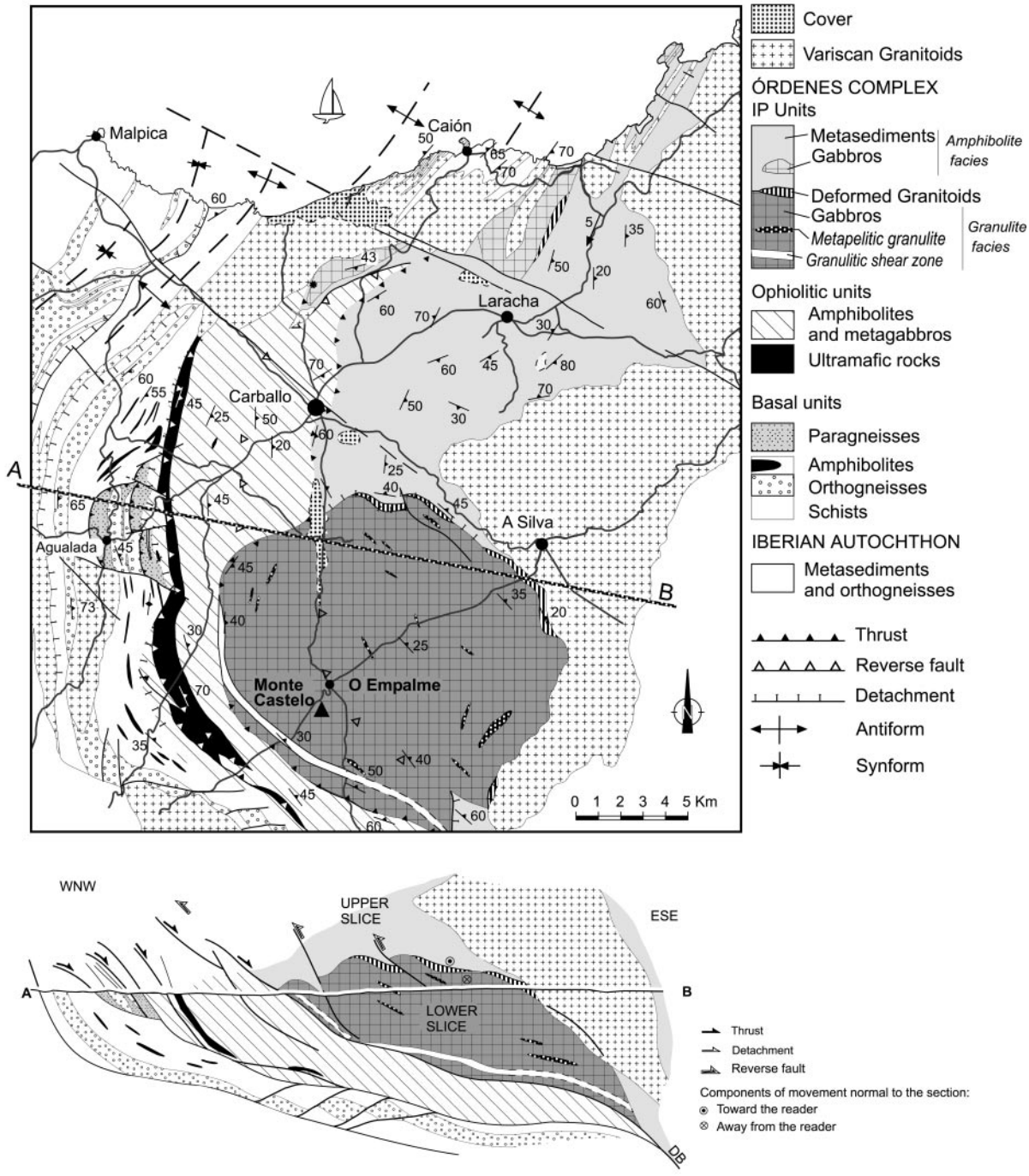

Fig. 2. Geological map and cross-section of the Monte Castelo area, with indication of the main outcrops of granulitic rocks inside the Monte Castelo Gabbro (dark grey with orthogonal grid). (For location, see Fig. 1.)

below). Hence, the metamorphism of these enclaves is linked in this study with the prograde metamorphism that affects the MCG.

The mafic granulites are mainly found in a shear zone that can be followed through the basal part of the MCG (Fig. 2), near its western and SW limits, with a thickness

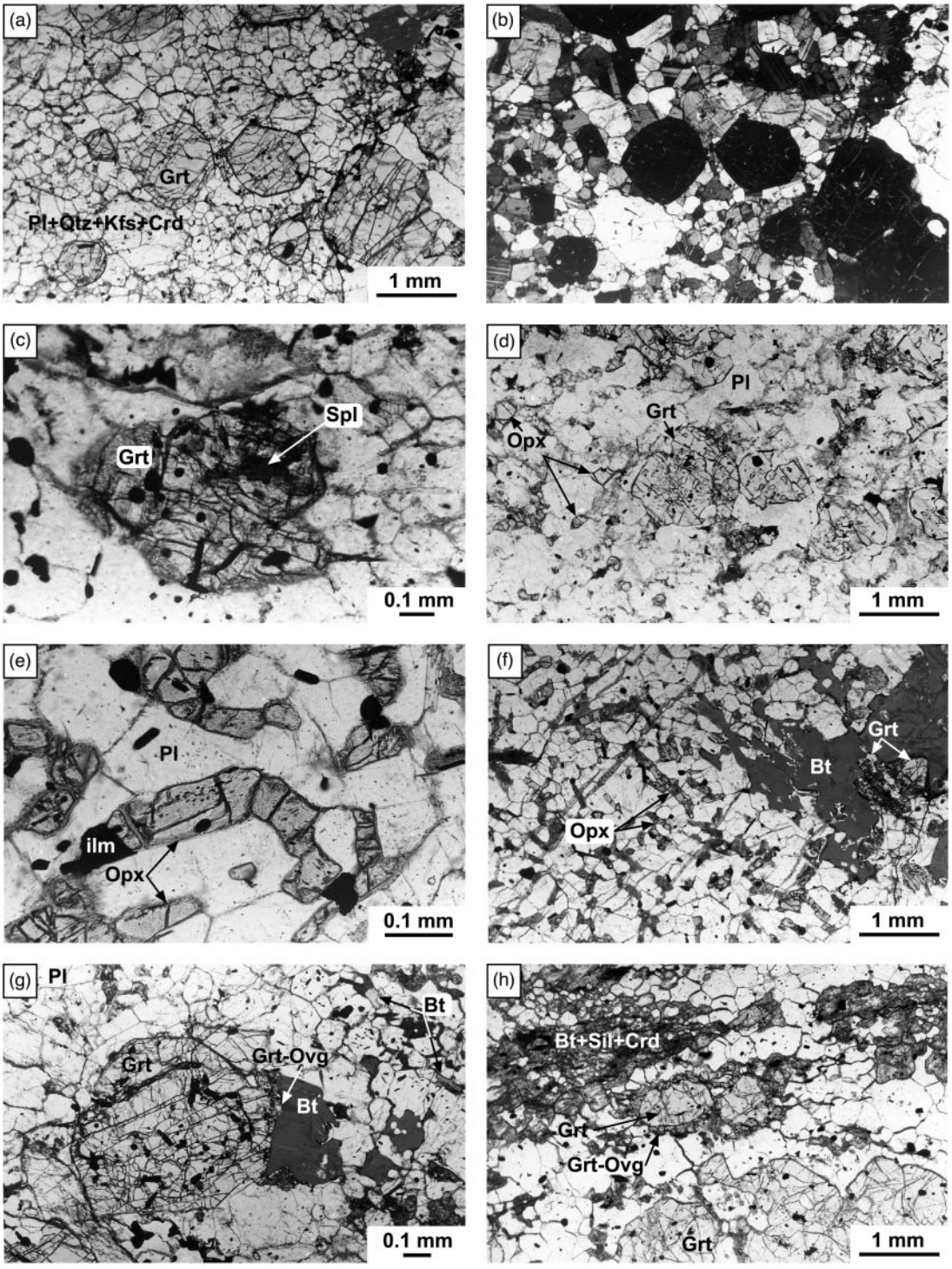

Fig. 3. Photomicrographs showing key characteristics of the metapelitic granulites: (a)–(e), granoblastic granulites; (f)–(h), biotite granulites. Textural relationships of the aluminous leucosomes characteristic of the granoblastic granulites are shown in (a)–(c); garnets in these aggregates are typically idiomorphic or subidiomorphic, and frequently exhibit micro-inclusions of ilmenite and spinel [see (c)]. The less aluminous compositional domains of the type-1 granulites, generally rich in garnet and orthopyroxene, are shown in (d) and (e); (e) depicts a detailed image of the orthopyroxene crystals forming part of these aggregates. Three examples of typical biotite granulites, frequently with large biotite–garnet intergrowths, are shown in (f)–(h). In these granulites, a new generation of garnet appears, forming overgrowths (Grt-Ovg) that surround the idiomorphic or subidiomorphic garnets of the type-1 granulites [(g) and (h)].

ranging between 50 and 200 m. Other minor, unmappable granulitic shear zones also exist. The shear zones resulted in a complete recrystallization of the igneous paragenesis, forming a new metamorphic mineral assemblage consisting of garnet, orthopyroxene, biotite, plagioclase, quartz, ilmenite and rutile, arranged in granoblastic to grano-nematoblastic textures. In the most deformed domains, the granulites exhibit a millimetre- to centimetre-scale banding defined by the alternation of garnet–pyroxene- and plagioclase–quartz-rich domains. In detail, the foliation is defined by the planar orientation of pyroxene and plagioclase, in addition to the previously mentioned banding. Frequently, the high-T foliation evolves to a more penetrative amphibolite-facies foliation formed by hornblende, garnet, plagioclase, quartz and ilmenite. The foliation trend is parallel to the western limit of the MCG, dipping 20–45°E.

PETROGRAPHY

Aluminous granulites

The aluminous granulites are medium- to coarse-grained rocks with textures varying from granoblastic, in the little deformed central part of the MCG, to porphyro-nematoblastic in the most deformed domains. The widespread occurrence of partial melting, together with a complex textural and mineralogical evolution explain the heterogeneous character of the aluminous granulites. This heterogeneity is always obvious, and can be observed in each outcrop and even in most thin sections. Three types of aluminous granulites, representative of three metamorphic stages of the same P–T path, have been distinguished: (1) granoblastic granulites; (2) biotite granulites; (3) retrogressed granulites.

Two types of compositional domains can be recognized in the granoblastic granulites of type 1. These domains, which can alternate even in a single thin section, are characterized by different Al_2O_3 contents and show distinct mineral assemblages. The more aluminous domains are leucosomes with a mineral assemblage formed by quartz, plagioclase, orthoclase, cordierite, garnet, ilmenite and green spinel (Fig. 3a–c). They appear as granoblastic aggregates where the garnet porphyroblasts are the larger crystals. Garnets in these aggregates are typically idiomorphic or subidiomorphic, exhibit sharp contacts with the other minerals and frequently have a poikiloblastic character, with microinclusions of ilmenite and spinel. The latter minerals also exist in the granoblastic matrix surrounding the garnets, where some rounded grains of spinel can reach 1 mm. Cordierite crystals are scarce and occasionally may be absent in some samples. The less aluminous compositional domains contain quartz, plagioclase, orthoclase, orthopyroxene, garnet, ilmenite and scarce cordierite. In these domains, orthopyroxene crystals appear as grey to pinkish idiomorphic or subidiomorphic prisms of <1 mm, either with a random distribution or forming a grano-nematoblastic fabric, showing sharp contacts with the other minerals (Fig. 3d and e). Garnets have characteristics similar to those described in the more aluminous domains, but they contain exclusively microinclusions of ilmenite. As will be discussed below, garnets from the type-1 granulites are mainly homogeneous in composition, although some crystals exhibit a significant increase in CaO content in the last 15–20 μm.

The two compositional domains described in the type-1 granulites provide evidence of the significant migmatization that affected these lithologies. Partial melting coincided in time with the oldest metamorphic stage preserved in the P–T path, and probably occurred in relation to the metamorphic thermal peak. Considering the mineral assemblage preserved in the most common leucosomes, which will be discussed in a following section, the more important migmatization affecting the aluminous granulites occurred at relatively low pressure. After the most important migmatitic event, the progression of the P–T path was coeval with the development of the high-T foliation in the aluminous granulites. During this stage, the stability of the mineral assemblage including spinel was surpassed and the type-1 aluminous granulites developed a unique assemblage with garnet, orthopyroxene and cordierite.

Textural evidence clearly suggests that the biotite granulites of type 2 come from the recrystallization of the granoblastic granulites, and were therefore developed during a more advanced stage of the P–T path. The most characteristic minerals in these lithologies generally have a local development, and grow from the granoblastic aggregates characteristic of the type-1 granulites. The transition from the type-1 granulites to the biotite granulites has syntectonic characteristics, and generally occurred without a complete texture reconstruction. Thus, it can be observed how the granoblastic or grano-nematoblastic mosaics of the type-1 granulites were affected by local recrystallization limited to specific microdomains, where the mineral assemblages characteristic of the type-2 granulites developed. This textural evolution to type-2 granulites, which frequently preserved little-modified domains of type-1 granulites, clearly suggests that the P–T path did not evolve to higher temperatures. This interpretation is also substantiated by the P–T conditions that can be calculated for the mineral assemblage characteristic of the biotite granulites.

The mineral assemblage of the biotite granulites consists of quartz, plagioclase, orthoclase, biotite, garnet, orthopyroxene, rutile and scarce cordierite (Fig. 3f–h). A new generation of garnet appears, forming overgrowths that surround the idiomorphic or subidiomorphic garnets of the type-1 granulites (Figs 3h and 4a and b). These

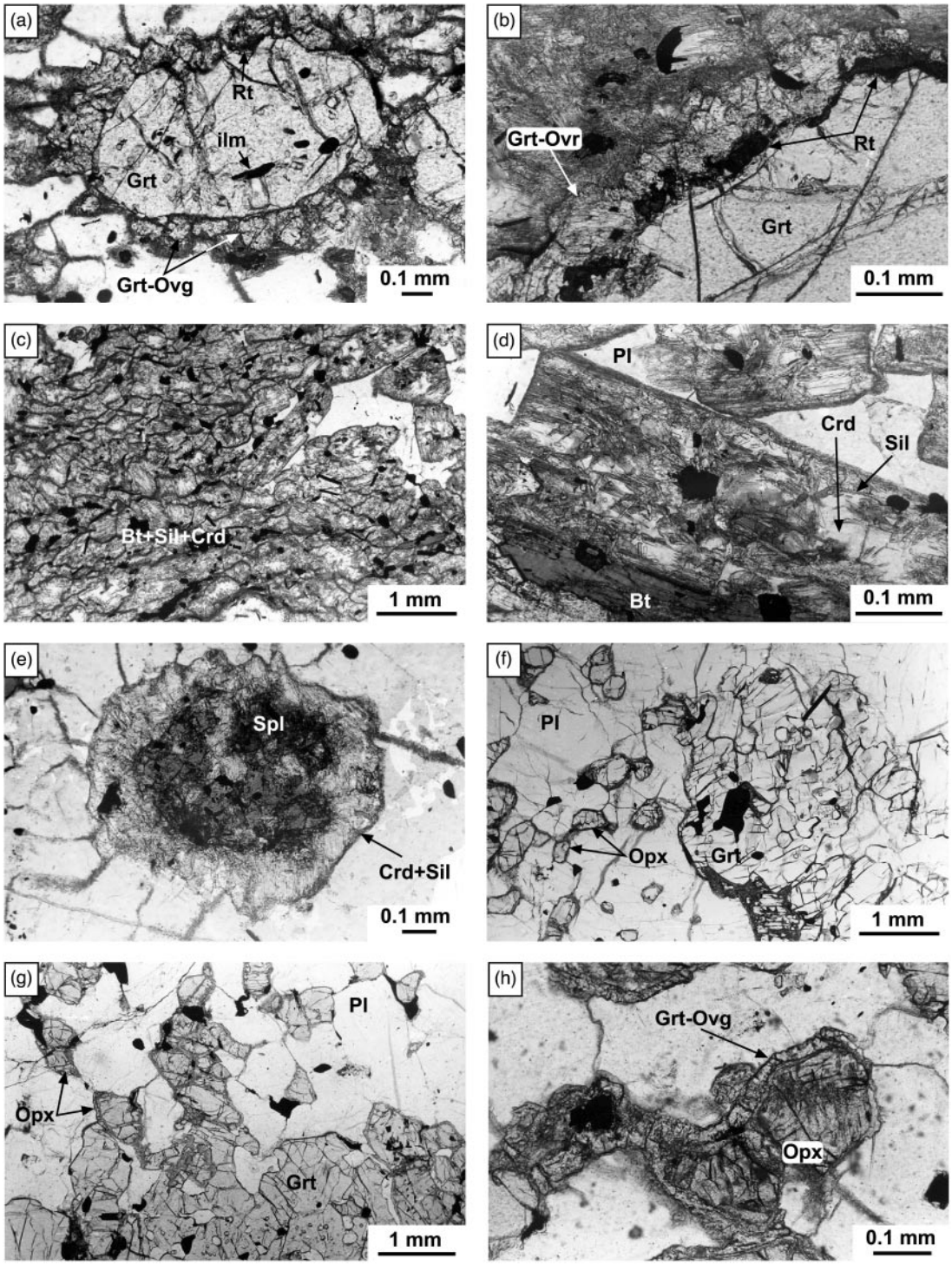

Fig. 4. Photomicrographs showing key characteristics of the metapelitic granulites [(a) and (b), biotite granulites; (c)–(e), retrogressed granulites] and mafic granulites (f)–(h). (a) and (b) show two examples of garnet overgrowths (Grt-Ovg) surrounding older garnet crystals; the development of many rutile grains in the contact area between the two types of garnet can be observed in (b). (c)–(e) show textural aspects of the retrogressed granulites. Mineral aggregates mainly constituted by retrogressed orthopyroxene crystals can be observed in (c); in these aggregates, individual orthopyroxene grains have been completely replaced by biotite, cordierite and fibrolitic sillimanite (d). The latter two minerals also form retrogressive coronas around previous crystals of green spinel (e). (f) and (g) show the textural aspect of the mafic granulites, with granoblastic or grano-nematoblastic aggregates mainly consisted of garnet, orthopyroxene, plagioclase, quartz, ilmenite and rutile. Fine garnet coronas surrounding granoblastic orthopyroxenes of a previous metamorphic stage can be observed in (h).

overgrowths have higher contents in CaO and MgO than the previous garnets, and generally show abundant microinclusions of rutile frequently developed in the contact area between the two types of garnets (Fig. 4b). Small garnets or aggregates of allotriomorphic garnets may also appear, forming intergrowths with biotite, or surrounding large porphyroblastic crystals of high-T reddish biotite (Fig. 3f and g). The development of the biotite–garnet intergrowths occurred, at least in a first stage, with stability of orthopyroxene in the mineral assemblage of the type-2 granulites. Orthopyroxene is a characteristic mineral in the biotite granulites, although it can be absent in samples where cordierite has an important modal content.

In many of the granulite samples studied, the assemblages characteristic of types 1 and 2 were affected by an important retrogression. Taking into account the new mineral assemblages developed in the retrogressed types, this retrogression occurred at high temperature. The retrogressed granulites of type 3 contain quartz, plagioclase, orthoclase, biotite, garnet, sillimanite and cordierite. In the most characteristic lithologies of this group, the orthopyroxene crystals developed previously appear completely replaced by a fine-grained aggregate of fibrolitic sillimanite, biotite and cordierite (Fig. 4c). The shape of the orthopyroxene crystals can be perfectly recognized, because the limits of individual grains appear generally defined by the mimetic growth of fine needles of sillimanite (Fig. 4d). The mineral assemblage including sillimanite, biotite and cordierite is the last one developed in type-3 granulites. The development of coronas with cordierite and sillimanite surrounding some previous crystals of green spinel (Fig. 4e) can also be assigned to this stage of high-T retrogression. Moreover, the type-3 granulites do not contain muscovite, which can be considered as additional evidence for their high-T origin.

Reaction history and *P–T* path

Several petrogenetic grids have been proposed for pelites in the melting region (Powell & Downes, 1990; Carrington & Harley, 1995; Thompson and Connolly, 1995; Spear *et al.*, 1999). The petrogenetic grid presented by Spear *et al.* (1999) is highly appropriate for investigating phase relations in the aluminous granulites studied, and has been used to establish the P–T path followed by these rocks (Fig. 5).

Two mineral assemblages were initially developed in the granoblastic granulites. The minerals forming part of these parageneses are the oldest phases observed in the aluminous granulites. One of the assemblages is restricted to the aluminous leucosomes (Spl + Grt + Crd + Qtz + Pl + Kfs + Ilm), whereas the other is preferentially developed in the nematoblastic domains (Opx + Grt + Crd + Qtz + Pl + Kfs + Ilm). Both mineral assemblages are divariant in the NKFMASH system, and their presence clearly suggests that the P–T path enters field VI (Fig. 5). Considering that the more characteristic leucosomes contain the mineral assemblage with spinel, it is reasonable to assume that the more important melt crystallization occurred in this field.

In the granoblastic granulites, the progressive development of the high-T foliation involved the destabilization of the assemblage with spinel. The aluminous granulites, strongly deformed at high T, show a penetrative foliation characterized by the presence of frequent nematoblastic layers with many prismatic orthopyroxene crystals. The alternating granoblastic layers generally contain cordierite, garnet and some orthopyroxene, but they do not contain spinel. This fact clearly suggests that the development of the high-T foliation was associated with an important pressure increase, coeval with the replacement of the assemblage with spinel by another divariant assemblage consisting of Opx + Grt + Crd + Qtz + Pl + Kfs + Ilm. This mineral assemblage was probably the only one present in the aluminous granulites during this stage of their P–T evolution. Considering that this stage occurred after the destabilization of the mineral assemblage with spinel, its development was probably related to the crossing of the P–T path across field V (Fig. 5). On the other hand, the aluminous granulites never contain the mineral assemblage characteristic of field VII (Opx + Grt + Sil + Qtz + Pl + Kfs; Fig. 5). As will be discussed in a following section, this fact, together with the succession of mineral assemblages developed in the aluminous granulites, suggests that the final evolution of the P–T path occurred towards lower temperatures than those characteristic of field VII.

Two divariant mineral assemblages are characteristic of the biotite granulites: (1) Opx + Grt + Bt + Qtz + Pl + Kfs + Rt; (2) Grt + Bt + Crd + Qtz + Pl + Kfs + Rt. Both assemblages are characteristic of field IV (Fig. 5), the first being the more frequent in the granulites described. The stabilization of these assemblages occurred during the progressive development of the high-T foliation. This is another reason why the P–T path characteristic of these granulites shows a drastic and almost isothermal pressure increase. This path finally entered into field III, where two new mineral assemblages developed (retrogressed granulites; Fig. 5). One of these assemblages is probably older, and consists of Grt + Bt + Sil + Qtz + Pl + Kfs + Rt. The textural relationships of this assemblage suggest that it was stabilized during the last stages in the development of the high-T foliation. The second mineral assemblage is the most common in the retrogressed granulites, and consists of Bt + Crd + Sil + Qtz + Pl + Kfs. Biotite, cordierite and sillimanite

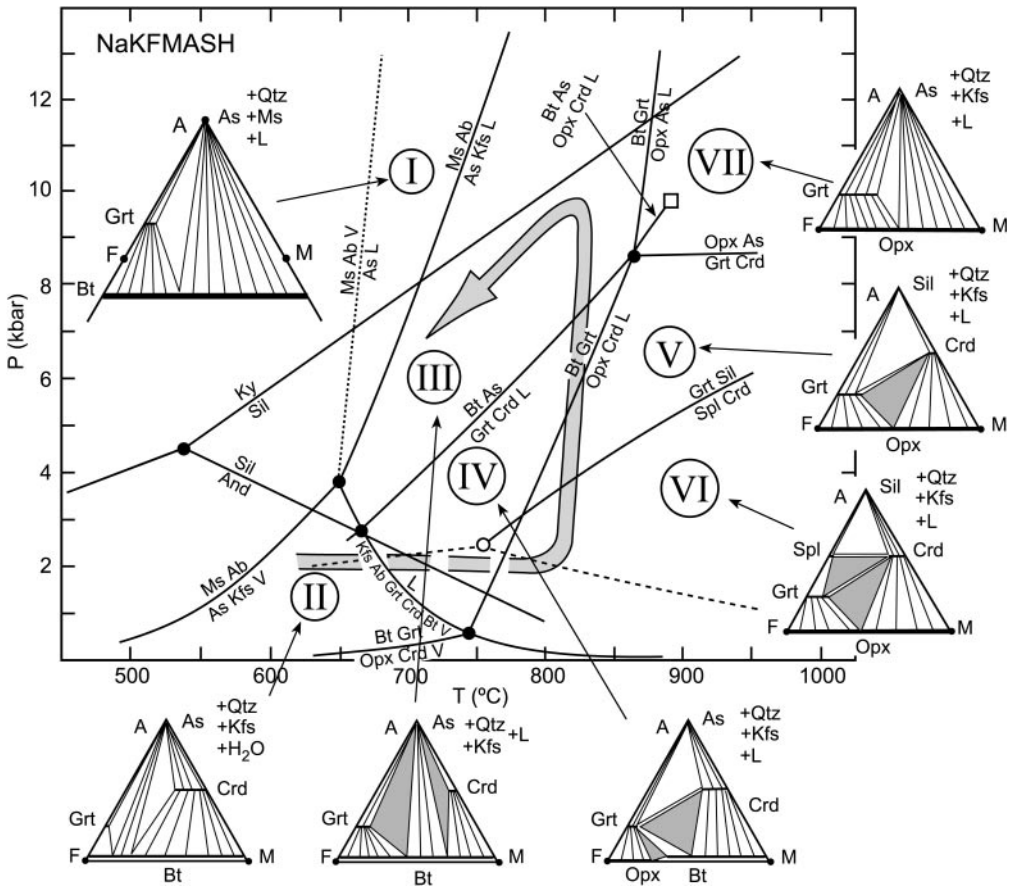

Fig. 5. *P–T* path suggested for the metamorphic evolution of the aluminous granulites included in the Monte Castelo Gabbro. AFM diagrams with the divariant assemblages of the aluminous granulites are also shown (shaded fields). Type-1 granulites (granoblastic granulites) developed in fields VI and V, whereas type-2 granulites (biotite granulites) developed when the path crossed fields IV and III, following an isothermal pressure increase. The development of the type-3 granulites (retrogressed granulites) coincided with the first stages of exhumation and cooling across field III. The petrogenetic grid for the NaKFMASH system is from Spear *et al.* (1999).

appear forming pseudomorphic intergrowths after orthopyroxene. With the exception of the occasional low-T retrogression observed in some samples, the stabilization of an assemblage without garnet represents the last mineral change observed in the aluminous granulites.

According to the petrogenetic grid used (Fig. 5), the development of a succession of mineral assemblages characteristic, in chronological order, of the fields VI, V, IV and III, is compatible only with a *P–T* path characterized by a drastic and almost isothermal pressure increase. On the other hand, the final high-T retrogression characteristic of this *P–T* path (mineral assemblage with Bt + Crd + Sil + Qtz + Pl + Kfs) suggests that its geometry is anticlockwise, and that the *P–T* loop experienced final exhumation and cooling across field III.

As has been described in a previous section, one of the most important characteristics of the aluminous granulites is the development of a second generation of garnet. The new garnets form overgrowths over the previous idiomorphic–subidiomorphic garnets, and are homogeneous in composition, typical of the granoblastic granulites. The garnet overgrowths have higher contents of CaO and MgO than the first garnets, and coexist with biotite, orthopyroxene, cordierite and sillimanite. Both the textural relationships and the coexisting mineral assemblages suggest that these overgrowths developed in the last stages of compression and hence their growth must be mainly coincident with the baric peak of the *P–T* path. The thermobarometric data presented below are also in agreement with this interpretation. On the other hand, the relatively high CaO contents of the garnet overgrowths are also compatible with an increase in pressure, and with progressive crossing of the isopleths with positive slopes of the GASP equilibrium (3 anorthite = grossular + Al_2SiO_5 + quartz). Moreover, the MgO increase in the garnet overgrowths is also consistent with this interpretation, and compatible with the general

geometry of the Fe/(Fe + Mg) isopleths in garnets from different metapelitic assemblages at intermediate and high T (Spear *et al.*, 1999). The development of the garnet overgrowths could be associated, at least in a first stage, with the passing of the P–T path into field IV (Fig. 5), where new growth of garnet can be produced by the reaction cordierite + orthopyroxene + K-feldspar + liquid = biotite + garnet + quartz (Spear *et al.*, 1999). It is not clear which reaction could explain the development of garnet overgrowths in field III, but in any case the coexistence of garnet and biotite is possible at least in the upper part of this field (Spear *et al.*, 1999).

Mafic granulites

Samples from the shear zones located in the basal part of the MCG are fine- to medium-grained granulites with grano-nematoblastic or porphyro-nematoblastic textures (Fig. 4f–h). The most common granulitic types contain porphyroblasts of garnet and orthopyroxene, surrounded by a granoblastic or grano-nematoblastic matrix consisting of orthopyroxene and plagioclase, with lower contents of quartz, biotite, ilmenite and rutile. The retrogressed types also contain variable amounts of hornblende, clinozoisite, chlorite, sphene and epidote.

A striking feature of these granulites is the absence of clinopyroxene. In mafic granulites of basaltic composition (*sensu lato*), clinopyroxene–orthopyroxene is a characteristic association at low to intermediate pressures, and orthopyroxene becomes unstable as the pressure increases. As the protolith of these granulites, the MCG, has a typical tholeiitic composition (Andonaegui *et al.*, 2002), some change in the bulk chemical composition should be invoked to explain the stability of the association Opx + Grt + Pl without Cpx, which is characteristic of these rocks. This granulitic assemblage can be stable only for protolith compositions with a relatively high Fe/(Fe + Mg) ratio and moderately poor in Ca (e.g. Spear, 1993). Hence, we favour the hypothesis that some local metasomatism occurred in the MCG during metamorphism, probably related to the circulation of fluids during shearing, to explain the absence of clinopyroxene. In any case, the characteristics of the metasomatic process do not affect the thermobarometric estimations.

In spite of their different chemical composition, the mafic granulites developed a succession of textures and assemblages very similar to that of the aluminous granulites. The oldest mineral assemblage preserved in the mafic granulites consists of garnet, orthopyroxene, plagioclase, quartz and ilmenite. The garnets are pale pink, up to 4–5 mm in diameter, and show an idiomorphic or subidiomorphic shape. They usually contain microinclusions of the other minerals forming part of this first assemblage (orthopyroxene, plagioclase, quartz and ilmenite; Fig. 4f and g). Orthopyroxene crystals are grey to pinkish, up to 3 mm long, and generally subidiomorphic. In the retrogressed types, the orthopyroxene crystals are replaced first by brown hornblende and later by green hornblende. Plagioclase and quartz form granoblastic or slightly oriented mosaics, with a variable size up to 1 mm.

The first metamorphic stage observed in the mafic granulites is contemporary with the initial development of a high-T foliation. The origin of this foliation is related to the shear zones developed in the basal part of the MCG (see Fig. 2). According to its metamorphic and textural characteristics, together with the thermobarometric data that will be presented below, the first mineral assemblage developed was essentially contemporary with the type-1 aluminous granulites (granoblastic granulites). Hence, it probably reveals similar P–T conditions to those of the metapelitic path during its transition across fields VI and V (Fig. 5). Nevertheless, the mafic granulites do not show any evidence of partial melting.

During a second metamorphic stage, the idiomorphic–subidiomorphic garnets of the granoblastic aggregates developed fine overgrowths of new anhedral garnet. Small rutile grains grow inside the overgrowths, as well as in the contact area between the old garnets and the overgrowths. Fine garnet overgrowths also appear, forming coronas around orthopyroxene crystals characteristic of the previous granoblastic aggregates (Fig. 4h), as well as intergrowing with large biotite crystals, up to 3 mm long, which exhibit characteristic deep reddish brown pleochroism, indicative of high Ti contents. As in the case of the oldest mineral assemblage preserved in the mafic granulites, it is also possible to correlate the assemblage with garnet overgrowths, orthopyroxene and biotite with its equivalent in the aluminous granulites. Hence, this metamorphic stage in the mafic granulites must be contemporary with the development of the type-2 aluminous granulites (biotite granulites), and linked to the development of an isothermal P–T path with a drastic increase in pressure.

The retrogressive evolution of the mafic granulites is marked by a succession of minerals developed at progressively lower temperatures. A first retrogressive stage characterized by the presence of brown hornblende was followed by a new metamorphic stage with green hornblende, and by a final one with chlorite, epidote–clinozoisite and sphene.

MINERAL CHEMISTRY

Most mineral analyses were performed using a Jeol JXA-8900 M electron microprobe equipped with four spectrometers at the Universidad Complutense de

Madrid, and a small number in a Cameca SX50 electron microprobe at the Universidad de Oviedo. The operating parameters were: 10 s counting time, 15 kV accelerating voltage, 20 nA beam current and a beam diameter between 2 and 5 μm. The ZAF correction procedure was used.

Garnet

Garnets of the aluminous (types 1 and 2) and mafic granulites were analysed, and X-ray maps and compositional profiles of the three types of garnets are shown in Figs 6–8. Figure 6 is an example of a subidiomorphic garnet from the leucosomes of the granoblastic granulites, Fig. 7 is a typical garnet with corona overgrowths from the biotite granulites, and Fig. 8 is a garnet from the mafic granulites.

Garnets of the granoblastic granulites are idio- to subidiomorphic, and almost chemically homogeneous, except for a very thin rim where growth zoning can be observed. The compositional variations of this zoned rim, from the inner to the outer part, are a slight decrease in pyrope and spessartine content, a moderate decrease in almandine content and, more important, an abrupt increase in grossular content, with maximum enrichment recorded in the outermost rim. The Fe/(Fe + Mg) ratio is generally slightly increased towards the rim, although some rims display the opposite trend, apparently with no relation to which mineral is in contact with garnet (Fig. 6). Garnets of the biotite granulites are usually characterized by the presence of an idiomorphic or subidiomorphic and homogeneous core surrounded by a xenomorphic overgrowth of variable thickness. These garnet rims also show growth zoning with Mn decrease towards the crystal border. The pattern is similar to that of the previous garnets with respect to Ca, Fe and Mn, but is different for Mg and the Fe/(Fe + Mg) ratio. The Mg content increases towards the rim, as occurs typically in growth zoning, and the Fe/(Fe + Mg) ratio decreases. This pattern also differs from the overgrowth-free garnets because the general trend of zoning is reversed in the outermost rim (Fig. 7).

Although distinct in composition, the garnets of the mafic granulites (Fig. 8) exhibit a zoning remarkably similar to the garnets of the granoblastic granulites, but with a wider zoned rim (Figs 6 and 8). These garnets are richer in Ca and poorer in Mg than garnets of the granoblastic granulites.

What follows from the above description is a pattern, common to the three types of garnets, consisting of an increase in grossular content towards the rims of the crystals, independently of the behaviour of the Fe/(Fe + Mg) ratio, which is more variable. Moreover, from X-ray maps it can be deduced that the zoning is not clearly related to which mineral is in contact with the garnet rim.

Some workers relate the increase in the grossular molecule in garnet rims to the secondary growth of Ca- and Mn-poor minerals, such as cordierite and biotite, at the expense of garnet (Tracy, 1982; Hand *et al.*, 1994). However, this does not seem likely in this case, because the rims of the garnets selected for the profiles are always in contact with quartz and plagioclase (Figs 6–and 8), and because their spessartine content shows a flat profile with a slight decrease in the rims, indicating that garnet is not reabsorbed. Furthermore, the identical zoning patterns between mafic and aluminous granulites suggest a similar evolution for both granulites. These relationships indicate that grossular content is not modified by secondary mineral growth (e.g. Baba, 1998). Hence the increase in grossular contents is related in this study to the growth of garnet rims and garnet coronas at higher-pressure conditions than the cores, which is also compatible with the textural study and petrogenetic grid data (see previous section). The complementary anorthite zoning of some of the plagioclases in contact with garnet (Fig. 9) is also compatible with a pressure increase during the last stages of garnet growth.

In summary, garnet zoning is interpreted as being produced in two steps: (1) diffusional homogenization as a result of high temperatures; (2) a subsequent overgrowth of garnets that preserve growth zoning essentially related to an increase in pressure. The preservation of the growth zoning may be favoured by a short time span of the burial–exhumation episode (e.g. Hiroi *et al.*, 1998). Similar trends of garnet zoning are scarce in the literature, but are generally interpreted in a similar way, that is, as a result of an abrupt increase in pressure (e.g. Erambert & Austrheim, 1993; Baba, 1998; Hiroi *et al.*, 1998).

The increase in Fe/(Fe + Mg) observed in some samples and the reversal of the zoning trend in the outer rims of garnets may reflect Fe–Mg re-equilibration associated with retrograde reactions.

Plagioclase

There are no significant chemical differences between matrix plagioclases and plagioclases included in other minerals (mainly garnet). Their composition is rather homogeneous, but there are important differences between plagioclases from mafic and aluminous granulites. Plagioclases from the former are relatively anorthite-rich, with a mean composition of An_{52}, whereas plagioclases from metapelites are around An_{36} (Fig. 10).

Matrix plagioclases show flat profiles, except when they are in contact with garnet, in which case they frequently show a significant An decrease in the last micrometres of the crystal rim (Figs 9 and 10). This

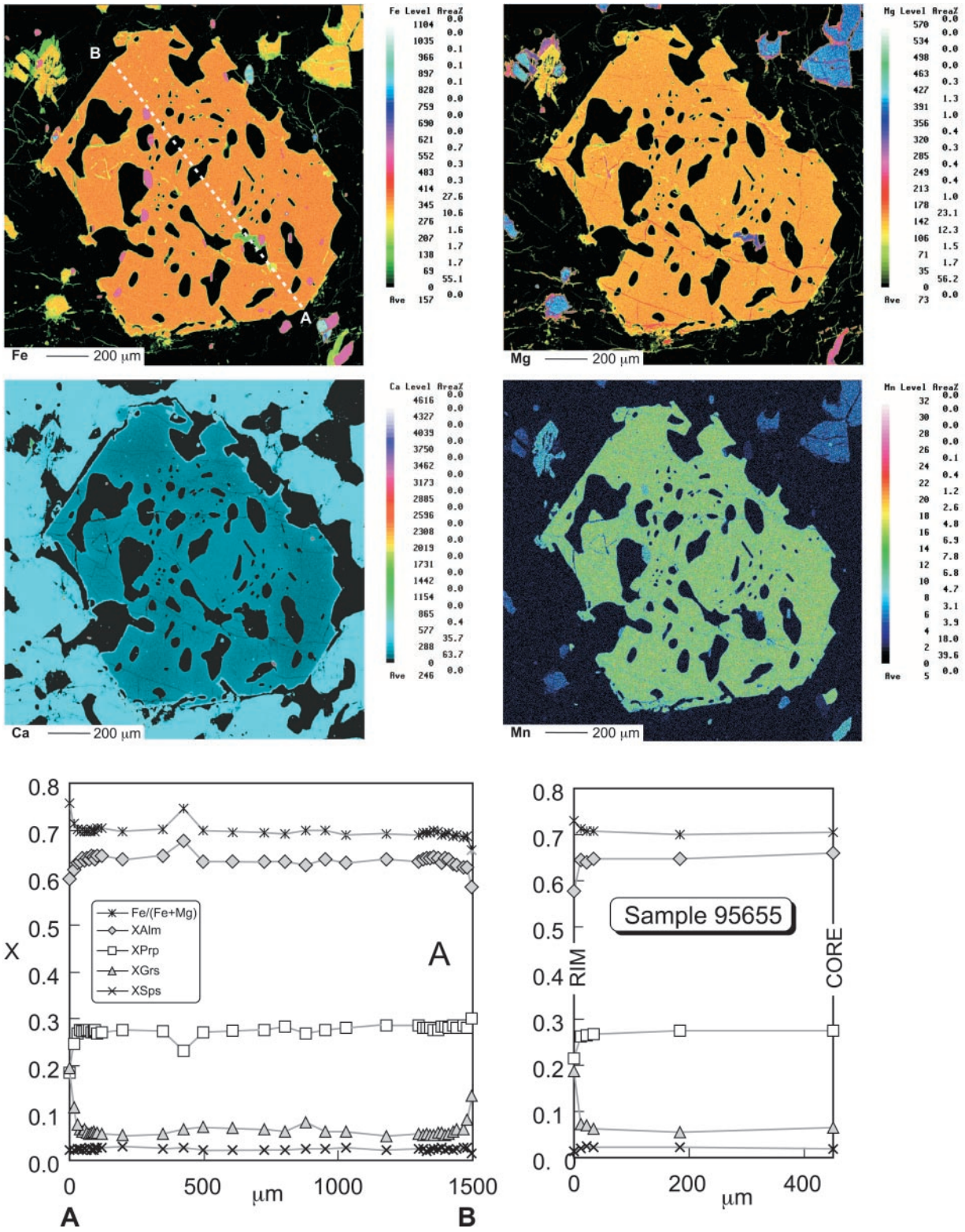

Fig. 6. X-ray maps and compositional profile of a garnet from the aluminous granulites. This is the typical garnet of the granoblastic (type-1) granulites (sample 99714), showing a poikiloblastic character with quartz and ilmenite inclusions. It is chemically homogeneous, except for a relatively Ca-rich thin rim with growth zoning. A semi-profile of a similar garnet from sample 95655 is also shown. The minerals in contact with garnet are plagioclase and quartz.

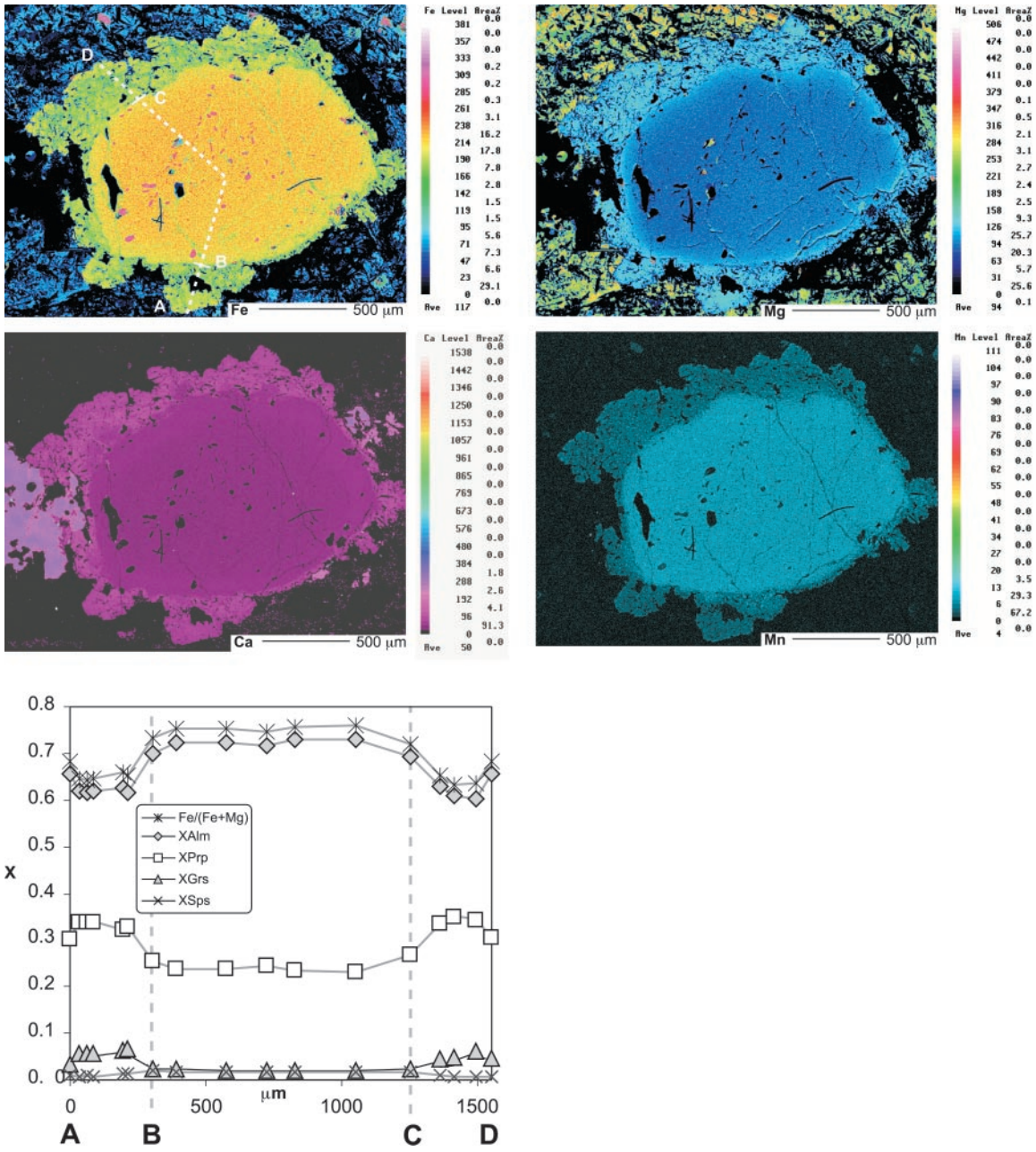

Fig. 7. X-ray maps and compositional profile of a garnet from the aluminous granulites. This is a representative garnet of the biotite (type-2) granulites with an idiomorphic core and a xenomorphic corona overgrowth. The corona is enriched in Ca and Mg and depleted in Fe and Mn with respect to the core, and at its extreme rim shows a reversal in the general trend of zoning, probably as a result of retrograde exchange reactions.

zoning pattern is antithetic to the Ca zoning of garnets (Fig. 9), and probably reflects An consumption to form the grossular component of garnets.

Orthopyroxene

Similarly to plagioclase, orthopyroxene is rather homogeneous and again there are significant chemical differences between orthopyroxenes from mafic and aluminous granulites. Matrix orthopyroxene from mafic granulites falls in the restricted compositional range Fs_{47-52}, and orthopyroxene from metapelites varies between Fs_{42} and Fs_{48} (Fig. 11). There are no observable compositional variations between the different textural types, such as orthopyroxene in contact or as inclusions in garnet, matrix orthopyroxene, etc. The Al_2O_3 content is higher

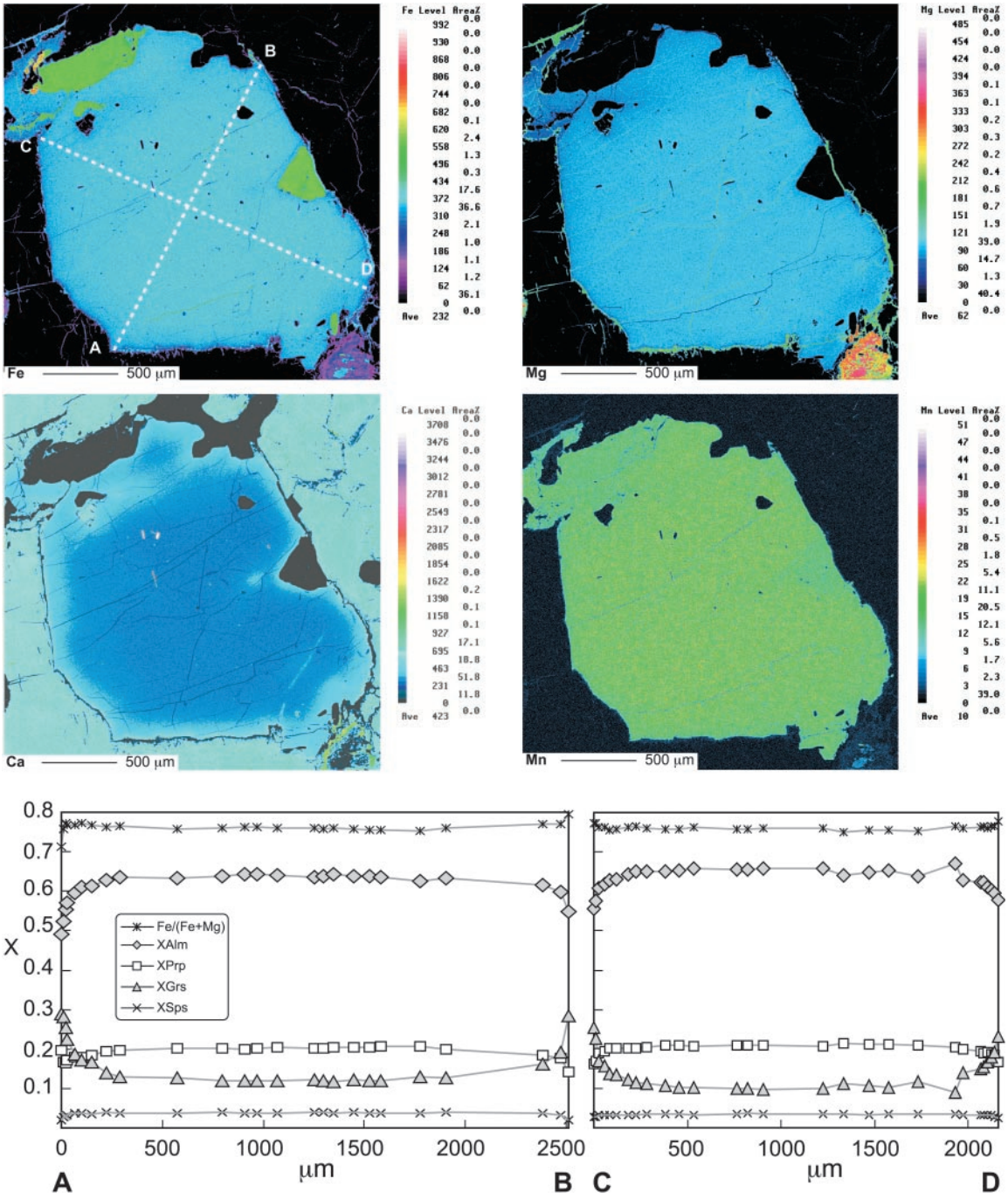

Fig. 8. X-ray maps and compositional profiles of a typical garnet from the mafic granulites. It should be noted that the zoning trend is almost identical to the garnet of the type-1 aluminous granulites, with Ca-rich and Fe- and Mg-depleted rims. The minerals in contact with garnet are plagioclase and quartz.

in the aluminous granulites (3–6%, vs 1–3% in mafic granulites) and the CaO content is slightly higher in mafic granulites. It is either unzoned or shows a slight zonation characterized by an increase in Fe/(Fe + Mg) and Al^{VI} (Fig. 11).

Biotite

Only biotites in textural equilibrium with the garnets of the biotite granulites were analysed. They are Ti rich (up to 6·5% TiO_2), which suggests a high crystallization temperature. Al^{VI} contents are relatively low, as is typical

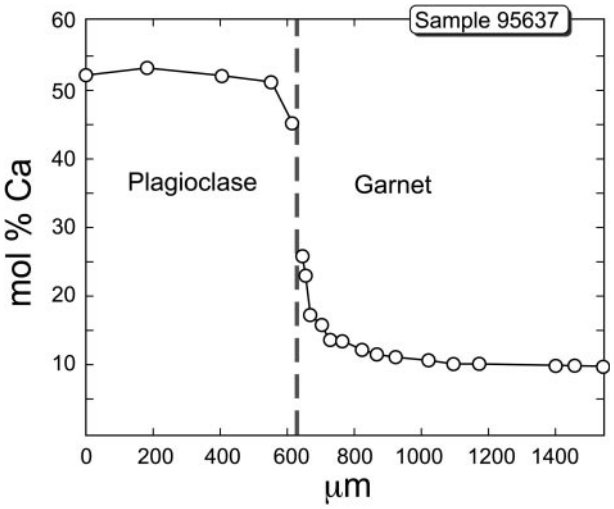

Fig. 9. Antithetic variation of Ca contents in a garnet and an adjacent plagioclase from sample 95637 (mafic granulite).

of high-grade metamorphic rocks. Biotites from metapelites are slightly richer in MgO and Al^{VI} than the biotites from mafic granulites (Fig. 12). They are generally unzoned, although some biotites in contact with garnet show a slight decrease in Fe/(Fe + Mg), indicating an exchange of Fe–Mg between both minerals.

Amphibole

Brown hornblende is homogeneous, with Fe/(Fe + Mg) ratios ranging from 0·4 to 0·5. Si (6·2–6·4 cations p.f.u.) and Ti contents (0·17–0·20 cations p.f.u.) are compatible with amphiboles generated in high-grade conditions.

Fe–Ti oxides

Fe–Ti oxides are ilmenite and rutile with very similar compositions in both types of granulites. Ilmenites have

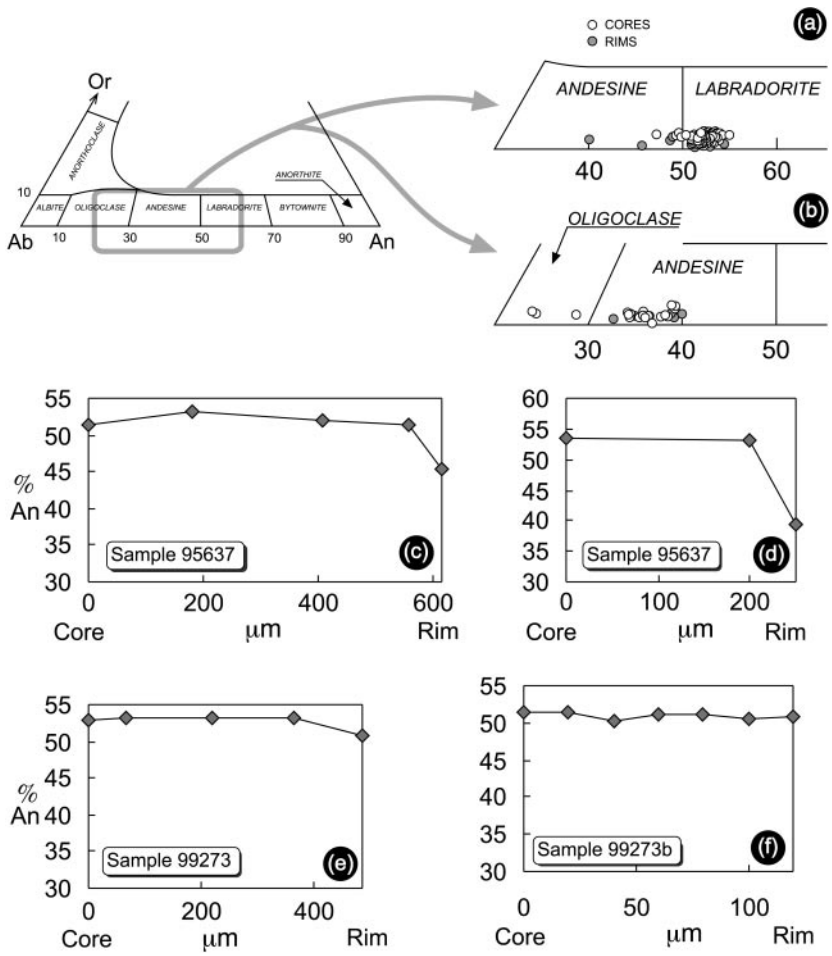

Fig. 10. Composition of the plagioclases from the granulites. (a, b) Classification of the plagioclases in the Ab–An–Or diagram; (a) mafic granulites, (b) aluminous granulites. (c)–(e) Variation of An content from cores to rims of plagioclases in contact with garnet. (f) Variation of An content in a plagioclase distant from garnet porphyroblasts.

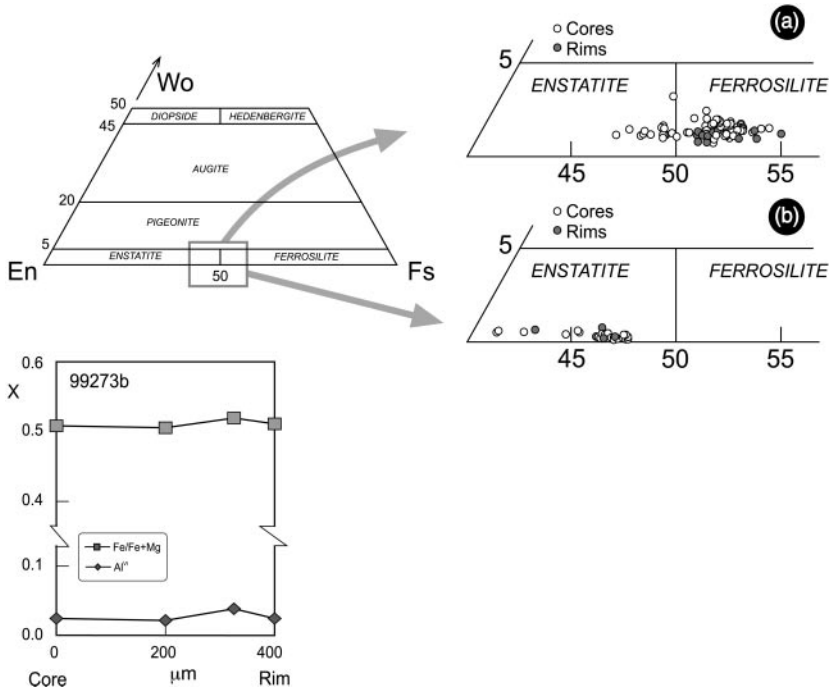

Fig. 11. Composition of orthopyroxenes from (a) mafic granulites and (b) aluminous granulites. In the lower part a representative semi-profile of one orthopyroxene is shown.

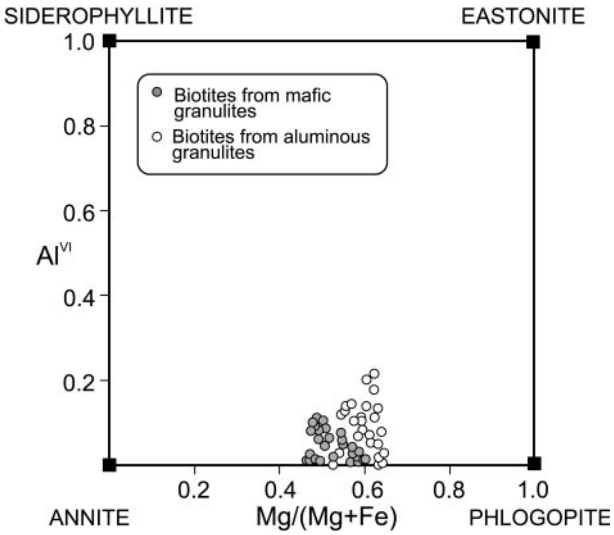

Fig. 12. Representation of the biotites in the Al^{VI} vs Mg/(Mg + Fe) diagram.

a composition of pure ilmenite end-member ($FeTiO_3$), variable between 92 and 96%. The other oxides correspond to rutile (2·1–5·2%), pyrofanite ($MnTiO_3$; 1·3–2·45%) and minor $FeAlO_3$ and $FeSiO_3$. Rutile corresponds to almost pure TiO_2 (97·7–99·9 TiO_2).

THERMOBAROMETRY

Mineral associations for thermobarometry were selected according to the textural and chemical study presented in the previous sections, and the temporal succession of parageneses is mainly based on the complex textural relationships of the aluminous granulites. Not all of the mineral assemblages described are useful for thermobarometry, because of their mineralogy (e.g. lack of garnet), or because some of them are limited to small domains probably not completely equilibrated. Therefore, the maximum thermobarometric information that we could obtain from these rocks is limited to two points of the *P–T* path.

Quantitative metamorphic *P–T* conditions were estimated using the multiequilibrium method TWQ (version 2.02; Berman, 1991; updated 1997), based on the internally consistent thermodynamic dataset of Berman (1988, 1991). The activity–composition models applied were from Berman & Aranovich (1996) for garnet and biotite, Fuhrman & Lindsey (1988) for plagioclase, and an ideal mixing model for pyroxene (Newton, 1983). Equilibria were calculated in the KCFMASH system using the end-members of garnet (grossular, pyrope, almandine), orthopyroxene (enstatite, ferrosilite), plagioclase (albite, anorthite), biotite (phlogopite, annite), K-feldspar and α-quartz.

One of the main advantages of multiequilibrium methods, when an adequate selection of mineral compositions is made based on a correct interpretation of textural relationships, is the possibility of assessing the state of equilibrium of a sample based on the dispersion of mutual intersections of independent equilibria for a given assemblage. The better the convergence of equilibria, the higher the probability of existence of chemical equilibrium in a given sample, whereas a great divergence indicates that one or more phases are not in mutual equilibrium (Berman, 1991; Lieberman & Petrakakis, 1991).

In our case, arithmetic means of selected analyses are probably more representative than individual analyses, taking into account the high compositional homogeneity of the minerals of these granulites. Therefore, to perform the thermobarometric calculations the arithmetic means were preferred.

Aluminous granulites

The oldest mineral phases observed in the aluminous granulites are in the textural domain described as granoblastic (type-1) granulites. Two mineral assemblages have been recognized, one restricted to the leucosomes (Spl + Grt + Crd + Qtz + Pl + Kfs + Ilm), whereas the other is preferentially developed in nematoblastic domains (Opx + Grt + Crd + Qtz + Pl + Kfs + Ilm). The first assemblage is not very well preserved, and very few spinel and cordierite analyses are available. The inclusion of these phases in the TWQ calculations produces a great dispersion of intersections, and it was not possible to obtain reliable *P–T* estimations. For the second assemblage, core compositions of garnets (both idiomorphic garnets of the granoblastic granulites and garnets with corona overgrowths of the biotite granulites) were combined with core compositions of matrix minerals (Opx, Pl). The compositions used for calculations are shown in Table 1. Cordierite was excluded from the calculations because it produced a great dispersion of equilibria. The intersection of the three possible reactions in the KCFMASH system (only two independent, hence it is not a multiequilibrium calculation) gives estimations of 782°C and 6·1 kbar for sample 99714, and 805°C and 4·6 kbar for sample 95655 (Fig. 13).

In some textural domains the granoblastic granulites are replaced by biotite granulites, with two characteristic mineral assemblages: (1) Opx + Grt + Bt + Qtz + Pl + Kfs + Rt; (2) Grt + Bt + Crd + Qtz + Pl + Kfs + Rt. Garnets of the biotite granulites were formed during a second stage of garnet growth, represented by thick overgrowths forming coronas around previous subidiomorphic crystals, and by the thin Ca-rich rims of the corona-free garnets. These garnet rim compositions were combined with rim compositions of matrix minerals (see Table 1), although there is no significant compositional variation from core to rim, except for some plagioclase rims in contact with garnet, which are more rich in albite (Fig. 9). The best results and convergence of equilibria are obtained for the first assemblage. Samples 99714 and 95655 show a very good convergence of equilibria (three independent reactions; see list of reactions in Table 2) intersecting at 824 $\pm$ 3°C and 8·4 $\pm$ 0·1 kbar, and at 824 $\pm$ 19°C and 8·3 $\pm$ 0·1 kbar, respectively (Fig. 13).

These *P–T* estimations suggest that the recrystallization of the granoblastic granulites to form the biotite granulites was accompanied by an almost isothermal pressure increase. The *P–T* variation deduced reproduces closely a fragment of the *P–T* path obtained using the petrogenetic grid for anatectic pelites (Fig. 14). However, the positions of the *P–T* points obtained for each mineral assemblage do not fall exactly within their stability fields as plotted in the petrogenetic grid. They are variably offset from their fields, and the *P–T* values for the granoblastic granulites (circles) plot in fields IV and V instead of falling within fields V and VI, whereas estimations for biotite granulites (squares) fall in field III instead of field IV (Fig. 14). Taking into account that the offset is not very important, we consider that this discordance can probably be attributed to the uncertainties in thermobarometry (especially in high-grade rocks) plus the uncertainties in the construction of the petrogenetic grid, and therefore we believe that the thermobarometric results reinforce the validity of the *P–T* path obtained using the petrogenetic grid.

Mafic granulites

As noted in the petrography section, the textural evolution of the mafic granulites is comparable with that of the aluminous granulites, and it is generally possible to correlate the distinct mineral assemblages with their equivalents in both granulites. The oldest mineral assemblage preserved in the mafic granulites consists of Grt, Opx, Pl, Qtz and Ilm, and is contemporary with the initial development of a high-*T* foliation, and is also probably coeval with the development of the type-1 aluminous granulites. A second metamorphic stage is mainly marked by garnet overgrowths forming coronas around orthopyroxene crystals, and intergrowing with large biotite crystals, which can be correlated with the type-2 aluminous granulites. The main paragenesis of the second stage consists of Grt, Opx, Bt, Pl, Qtz, Rt. Accordingly, TWQ thermobarometry was performed for the two metamorphic stages combining, for the first mineral assemblage, the composition of garnet cores with core compositions of matrix minerals and, for the second,

Table 1: Arithmetic means of mineral analyses from the aluminous granulites used for thermobarometry

Sample:	99714							95655						
	Type-1 granulites			Type-2 granulites				Type-1 granulites			Type-2 granulites			
	Grt	Opx	Pl	Grt	Opx	Pl	Bt	Grt	Opx	Pl	Grt	Opx	Pl	Bt
SiO_2	36·78	50·92	58·77	38·11	50·74	58·28	37·32	38·99	49·01	58·12	37·96	50·24	58·88	36·91
Al_2O_3	21·90	2·52	25·51	21·43	2·08	25·64	14·80	22·38	4·82	25·99	22·41	2·08	25·50	15·14
FeO	30·06	28·43	0·04	29·22	29·19	0·02	14·19	28·89	27·42	0·11	29·10	29·19	0·05	14·41
MnO	1·06	0·35	0·00	1·10	0·48	0·00	0·07	0·75	0·29	0·06	0·36	0·48	0·00	0·04
MgO	7·52	18·20	0·05	6·80	18·07	0·05	13·57	8·04	17·46	0·02	6·44	17·37	0·01	13·42
CaO	1·93	0·21	8·03	3·51	0·36	7·93	0·00	0·94	0·09	7·62	2·84	0·36	7·58	0·02
Na_2O	0·00	0·01	6·70	0·00	0·00	6·77	0·00	0·01	0·01	6·54	0·02	0·00	7·33	0·11
K_2O	0·00	0·00	0·23	0·01	0·02	0·22	10·04	0·00	0·00	0·13	0·00	0·02	0·18	9·81
TiO_2	0·00	0·04	0·04	0·09	0·03	0·03	5·30	0·02	0·10	0·01	0·01	0·03	0·03	4·83
NiO	0·09	0·01	0·00	0·03	0·00	0·02	0·09	0·00	0·02	0·00	0·00	0·00	0·02	0·04
Cr_2O_3	0·08	0·05	0·09	0·05	0·08	0·04	0·08	0·05	0·03	0·01	0·00	0·08	0·00	0·01
Total	99·43	100·74	99·46	100·35	101·05	99·00	95·46	100·07	99·25	98·61	99·14	99·85	99·58	94·74
n	14	9	8	2	2	2	3	22	11	18	2	3	3	2

n, number of individual analyses selected to calculate the mean.

garnet rims with rim compositions of matrix minerals (see compositions and list of reactions in Tables 3 and 4). The results are shown in Fig. 15, and they repeat a trend of pressurization similar to that shown by the aluminous granulites (Figs 13 and 14). However, T conditions for the rims are significantly higher than those obtained for the cores. This is probably due to an underestimate of the temperatures calculated for the first, less constrained, assemblage.

P–T PATH AND TECTONIC IMPLICATIONS

The *P–T* path for the granulites of the Monte Castelo Massif is depicted in Fig. 16. It records a first low-*P* heating followed by a dramatic pressure increase within the sillimanite field. Once the pressure peak was reached, it does not seem probable that the granulites remained in lower crust for a long time, because there is no evidence of isobaric cooling. Conversely, there is some evidence of decompression: (1) extensional detachments above the most important igneous bodies (González Cuadra *et al.*, 1999; Abati, 2000); (2) cordierite and plagioclase coronas around garnet in some samples of aluminous granulites, indicative of the reaction garnet + Al_2SiO_5 + quartz = cordierite; (3) presence of andalusite in the upper part of the uppermost unit, which probably had a final evolution in common with the lower part; (4) amphibolitization of mafic granulites accompanied by the transformation of rutile to ilmenite; (5) localized greenschist-facies shear zones.

The first part of the path in the aluminous granulites is related to their incorporation into the gabbro body as enclaves, resulting in intense heating (Fig. 16). The subsequent burial suggested by the path, up to 9 kbar, implies significant crustal thickening, which could be the result of massive magma injection into the crust (magmatic loading, Bohlen, 1987, 1991; Ellis, 1987; Harley, 1989), or may represent a tectonic loading, or a combination of these processes. The localization of granulites in prograde shear zones and the development of regional foliation suggest that the burial was, at least in part, tectonic.

However, simple models of continental collision cannot explain the type of *P–T* paths where the pressurization takes place at such high temperatures. This trend is consistent only with the magmatic accretion models first proposed by Bohlen (1987), where the supplementary heat contribution comes from intense igneous activity. This implies intense magmatism contemporaneous with crustal thickening, and points to an active margin that was undergoing magmatic underplating.

Similar trajectories have been related to magmatism at a continental margin followed by tectonic thickening (Appel *et al.*, 1998; Baba, 1998). The setting proposed

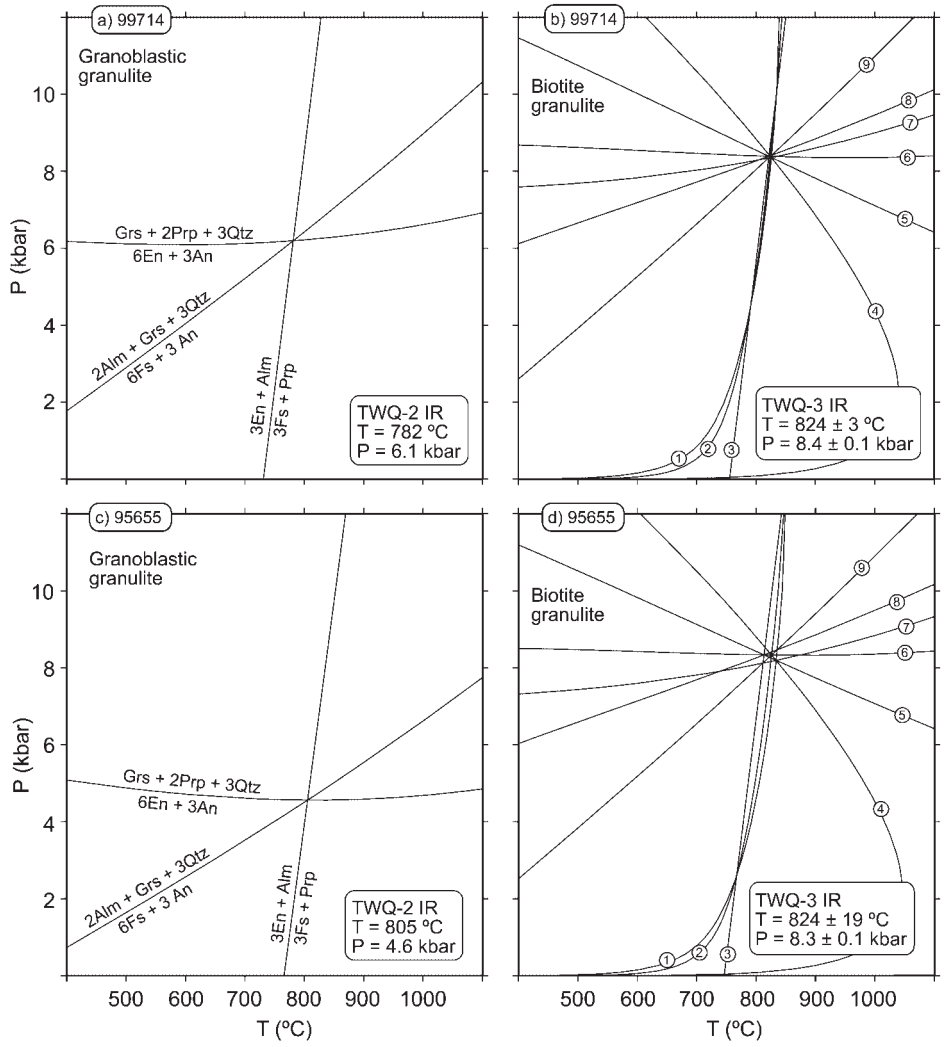

Fig. 13. *P–T* conditions estimated by the TWQ method for the aluminous granulites. Mineral compositions are given in Table 1 and list of reactions in Table 2.

Table 2: List of reactions for samples 99714 and 95655

(1)	3 βQtz + Phl = 3 En + Kfs + H_2O
(2)	Alm + Phl + 3 βQtz = Prp + Kfs + 3 Fs + H_2O
(3)	3 En + Alm = 3 Fs + Prp
(4)	Grs + 2 Kfs + 2 Prp + 2 H_2O = 3 βQtz + 2 Phl + 3 An
(5)	Grs + Kfs + 2 Prp + H_2O = Phl + 3 En + 3 An
(6)	Prp + Kfs + Grs + Alm + H_2O = 3 An + 3 Fs + Phl
(7)	Grs + 2 Prp + 3 βQtz = 6 En + 3 An
(8)	Kfs + 3 En + Grs + 2 Alm + H_2O = 3 An + 6 Fs + Phl
(9)	2 Alm + Grs + 3 βQtz = 6 Fs + 3 An

here for the origin of the granulites of the uppermost unit of the Órdenes Complex is the deep part of an accretionary prism generated in a magmatic arc, probably an island arc. The tectonic activity in this environment can explain all the characteristics of the uppermost unit and the deduced *P–T* path: the bimodal magmatism would derive from partial melting in the deep parts of the prism, as a result of the subduction of oceanic materials and associated sediments (Shiki & Misawa, 1982). The plutonic bodies generated in this way could be buried soon after their emplacement and incorporated into the accretionary prism. The dynamics of an accretionary prism also explains the existence of extensional processes simultaneous with the compressive activity (Platt, 1986). In addition to the characteristics of the *P–T* path, this interpretation is also supported by other

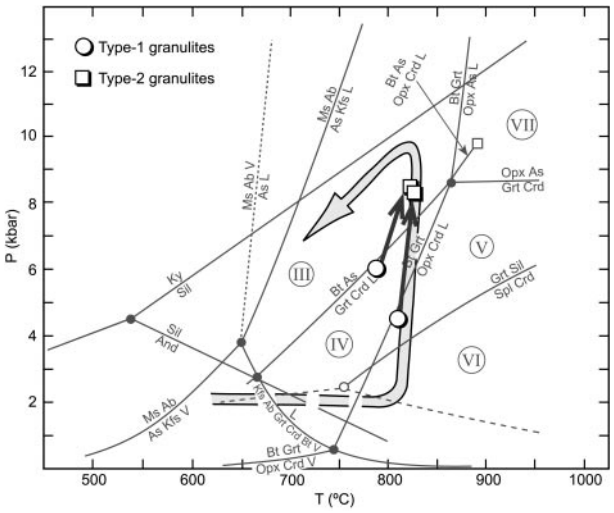

Fig. 14. Petrogenetic grid of Spear *et al.* (1999) showing the deduced *P–T* path for the aluminous granulites together with the quantitative *P–T* estimations obtained with the TWQ method. As can be seen, the *P–T* variation obtained with thermobarometry reproduces closely a fragment of the *P–T* path obtained using the petrogenetic grid. According to the petrogenetic grid, mineral assemblages of type-1 granulites should be formed mainly in fields V and VI, and those of type-2 granulites in field IV. However, the thermobarometric calculations based on the composition of the minerals of these assemblages are relatively displaced from their theoretical fields of stability. This is probably due to the uncertainties associated with thermobarometry in high-grade rocks and in the construction of petrogenetic grids.

Table 4: List of reactions for samples 99273b and 95637

(1)	2 Alm + Grs + 2 Phl + 3 βQtz = 6 En + 3 An + 2 Ann
(2)	3 En + Alm = 3 Fs + Prp
(3)	Alm + Phl = Prp + Ann
(4)	3 Fs + Phl = 3 En + Ann
(5)	3 βQtz + 2 Prp + Grs + 2 Ann = 3 An + 6 Fs + 2 Phl
(6)	Grs + 2 Prp + 3 βQtz = 6 En + 3 An
(7)	3 βQtz + Grs + 2 Alm = 3 An + 6 Fs

geological evidence: (1) the geochemistry of the mafic igneous rocks, specifically the MCG, indicates that they are tholeiites probably generated in an island-arc setting (Andonaegui *et al.*, 2002); (2) the almost syn-metamorphic character of the magmatism (Abati *et al.*, 1999) indicates that the emplacement of the plutons was immediately followed by their burial, which is a common feature of magmatic arcs (Bohlen, 1987; Hiroi *et al.*, 1998); (3) the sedimentary characteristics of the associated sediments (Órdenes Series), which are greywacke rich, turbiditic and very thick, are compatible with deposition in an area marginal to an island arc (Martínez Catalán *et al.*, 1999).

Table 3: Arithmetic means of mineral analyses from the mafic granulites used for thermobarometry

Sample:	99273b							95637						
	Type-1 granulites			Type-2 granulites				Type-1 granulites			Type-2 granulites			
	Grt	Opx	Pl	Grt	Opx	Pl	Bt	Grt	Opx	Pl	Grt	Opx	Pl	Bt
SiO_2	38·17	50·88	54·74	39·15	50·76	54·21	36·10	37·59	50·31	53·99	38·50	50·64	53·94	35·57
Al_2O_3	22·08	1·00	28·91	21·82	1·07	29·03	15·66	21·73	1·02	29·09	21·77	1·30	28·51	15·79
FeO	28·36	30·04	0·07	25·08	29·97	0·23	17·51	28·97	30·35	0·05	24·89	30·68	0·40	18·71
MnO	1·55	0·59	0·02	1·09	0·58	0·02	0·04	1·61	0·59	0·04	1·37	0·58	0·03	0·05
MgO	4·89	16·03	0·02	3·81	16·23	0·00	10·35	5·19	16·04	0·00	3·76	15·93	0·01	10·10
CaO	4·63	0·75	10·78	9·10	0·56	10·90	0·02	3·91	0·67	10·13	9·03	0·44	10·28	0·00
Na_2O	0·02	0·01	5·40	0·02	0·02	5·49	0·06	0·02	0·02	5·27	0·13	0·01	5·86	0·06
K_2O	0·00	0·00	0·23	0·00	0·00	0·14	8·58	0·01	0·00	0·27	0·00	0·00	0·10	9·17
TiO_2	0·03	0·08	0·01	0·03	0·06	0·02	5·92	0·05	0·07	0·02	0·01	0·03	0·02	5·12
NiO	0·04	0·03	0·03	0·04	0·05	0·04	0·02	0·03	0·04	0·02	0·03	0·02	0·00	0·01
Cr_2O_3	0·01	0·01	0·01	0·01	0·02	0·01	0·03	0·03	0·01	0·01	0·00	0·02	0·00	0·04
Total	99·80	99·41	100·20	100·20	99·32	100·10	94·30	99·14	99·13	98·88	99·49	99·65	99·15	94·63
n	19	18	24	3	5	15	6	21	17	19	4	7	5	4

n, number of individual analyses selected to calculate the mean.

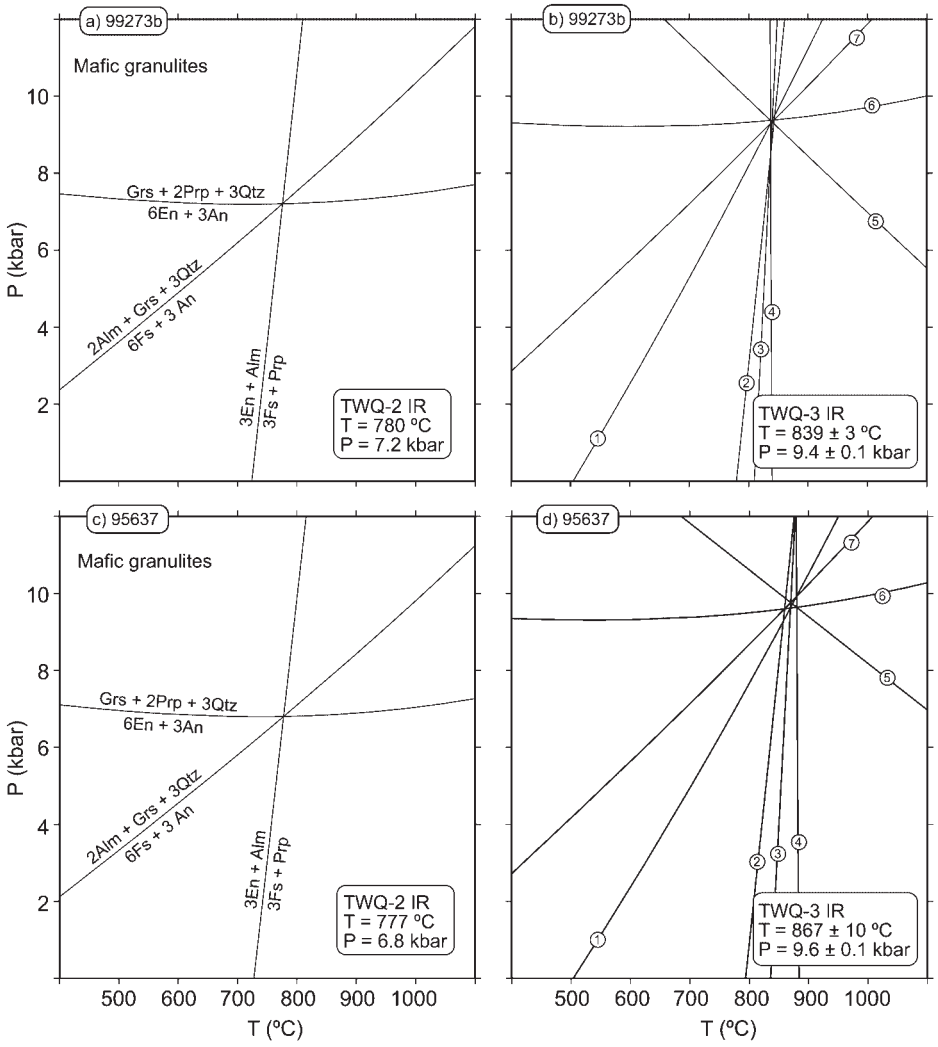

Fig. 15. *P–T* conditions estimated by the TWQ method for the mafic granulites. Mineral compositions are given in Table 3 and list of reactions in Table 4.

CONCLUSIONS

The mechanism generally invoked to explain zoning of the rims of homogeneous high-grade garnets is retrogressive diffusion as a result of post-peak cooling-driven reactions. However, the uncommon patterns of garnet zoning of the granulites from the Monte Castelo Gabbro suggest that the zoned rims can be produced by mechanisms other than retrogressive diffusion. In this case, it seems evident that the zoning responds to new garnet growth, as is indicated by the Mn decrease and the significant Ca increase from the inner to the outer rim. The possibility of preservation of growth zoning after high-grade conditions has been demonstrated by several workers (Tuccillo *et al.*, 1990; Indares, 1995; Chen *et al.*, 1998; Cooke *et al.*, 2000), and it is feasible when the rock undergoes only a short-term residence under high-grade conditions, precluding complete diffusion inside crystal volumes. This kind of zoning in granulites can yield information about the prograde history of high-grade rocks, which are generally obscured by the diffusional homogenization of minerals.

The *P–T* path obtained for the Monte Castelo granulites is very similar to other paths obtained in active plate margins (e.g. Appel *et al.*, 1998; Baba, 1998; Hiroi *et al.*, 1998), all of them characterized by a strong pressurization in the sillimanite field, and a subsequent, usually anticlockwise evolution (Fig. 16). A convergent margin is, therefore, the suggested setting for the origin of the granulites of the uppermost unit of the Órdenes Complex. According to the other geological features of the uppermost unit, the more probable type of convergent margin is an island arc.

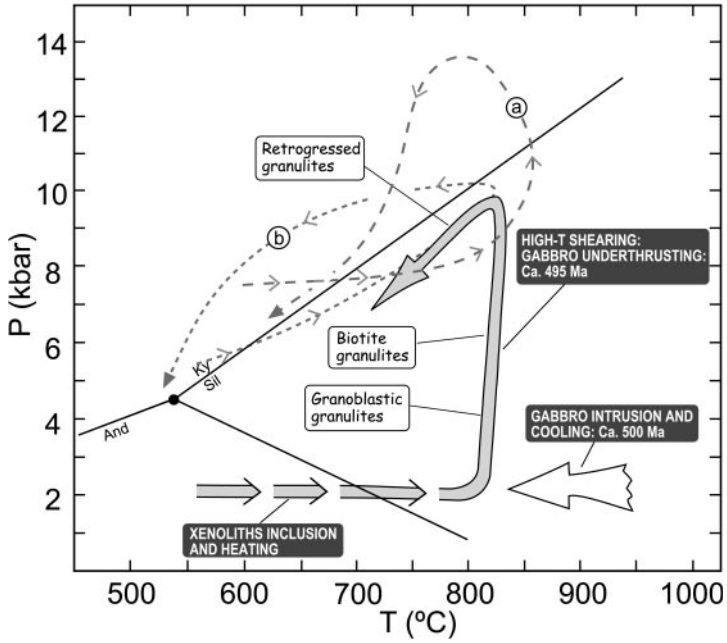

Fig. 16. Diagram showing the tectonothermal evolution of the Monte Castelo Gabbro and its aluminous inclusions. Gabbro intrusion at ~500 Ma (Abati *et al.*, 1999) was accompanied by the inclusion of many aluminous xenoliths. These xenoliths were strongly heated and probably melted during the progression of an almost isobaric *P–T* path. Shortly after intrusion (~495 Ma; Abati *et al.*, 1999), a high-*T* foliation developed in specific shear zones generated during gabbro underthrusting. The *P–T* path related to this underthrusting is restricted to the sillimanite stability field, and it is characterized by a quasi-isothermal increase in pressure. The last stages of foliation development coincided with the first exhumation and cooling of the gabbro massif. The metamorphic *P–T* path followed by the Monte Castelo Gabbro is anticlockwise, and hence very different from those characteristic of typical collisional orogenic belts. For comparison, two trajectories obtained in granulites related to terranes of intense magmatic injection are shown: (a) Baba (1998); (b) Appel *et al.* (1998).

The age of the granulitic metamorphism is ~495 Ma, approximately contemporaneous with the magmatism (~500 Ma; Abati *et al.*, 1999). The nearly syn-metamorphic character of the intrusions is also a common feature of magmatic arcs. Taken together, these data support the existence of a convergent plate boundary in a marginal area of Gondwana during the Late Cambrian–Early Ordovician times.

ACKNOWLEDGEMENTS

This research was funded by PB97-0234-CO2 and BTE 2001-0963-CO2 projects of the Spanish DGI. We would like to thank F. S. Spear, A. Indares and S. L. Harley for their constructive and helpful reviews, which significantly improved the quality of the manuscript. J. González del Tánago and A. Larios are thanked for their assistance with EPMA.

REFERENCES

Abati, J. (2000). Petrología metamórfica y geocronología de la unidad culminante del Complejo de Órdenes en la región de Carballo (Galicia, NW del Macizo Ibérico). Ph.D. thesis, Universidad Complutense de Madrid, 200 pp.

Abati, J., Dunning, G. R., Arenas, R., Díaz García, F., González Cuadra, P., Martínez Catalán, J. R. & Andonaegui, P. (1999). Early Ordovician orogenic event in Galicia (NW Spain): evidence from U–Pb ages in the uppermost unit of the Órdenes Complex. *Earth and Planetary Science Letters* **165**, 213–228.

Andonaegui, P., González del Tánago, J., Arenas, R., Abati, J., Martínez Catalán, J. R., Peinado, M. & Díaz García, F. (2002). Tectonic setting of the Monte Castelo Gabbro (Órdenes Complex, NW Iberian Massif): evidence for an arc-related terrane in the hangingwall to the Variscan suture. *Geological Society of America Special Paper*, **364** (in press).

Appel, P., Möller, A. & Schenk, V. (1998). High pressure granulite facies metamorphism in the Pan-African belt of eastern Tanzania: *P–T–t* evidence against granulite formation by continent collision. *Journal of Metamorphic Geology* **16**, 491–509.

Arenas, R., Gil Ibarguchi, J. I., González Lodeiro, F., Klein, E., Martínez Catalán, J. R., Ortega Gironés, E. Pablo Maciá, J. G. de & Peinado, M. (1986). Tectonostratigraphic units in the complexes with mafic and related rocks of the NW of the Iberian Massif. *Hercynica* **2**, 87–110.

Baba, S., 1998. Proterozoic anticlockwise *P–T* path of the Lewisian Complex of South Harris, Outer Hebrides, NW Scotland. *Journal of Metamorphic Geology* **16**, 819–841.

Berman, R. G. (1988). Internally-consistent thermodynamic data for minerals in the system Na_2O–K_2O–CaO–MgO–FeO–Fe_2O_3–Al_2O_3–SiO_2–TiO_2–H_2O–CO_2. *Journal of Petrology* **29**, 445–522.

Berman, R. G. (1991). Thermobarometry using multi-equilibrium calculations: a new technique, with petrological applications. *Canadian Mineralogist* **29**, 833–855.

Berman, R. G. & Aranovich, L. Y. (1996). Optimized standard state and solution properties of minerals (I). Model calibration for olivine, orthopyroxene, cordierite, garnet and ilmenite in the system FeO–MgO–CaO–Al_2O_3–TiO_2–SiO_2. *Contributions to Mineralogy and Petrology* **126**, 1–24.

Bohlen, S. R. (1987). Pressure–temperature–time paths and a tectonic model for the evolution of granulites. *Journal of Geology* **95**, 617–632.

Bohlen, S. R. (1991). On the formation of granulites. *Journal of Metamorphic Geology* **9**, 223–229.

Carlson, W. & Schwarze, E. (1997). Petrological significance of prograde homogenization of growth zoning in garnet: an example from the Llano Uplift. *Journal of Metamorphic Geology* **15**, 631–644.

Carrington, D. P. & Harley, S. L. (1995). Partial melting and phase relations in high-grade metapelites: an experimental petrogenetic grid in the KFMASH system. *Contributions to Mineralogy and Petrology* **120**, 270–291.

Chen, N. S., Sun, M., You, Z. D. & Malpas, J. (1998). Well-preserved garnet growth zoning in granulite from Dabie Mountains, central China. *Journal of Metamorphic Geology* **16**, 213–222.

Cooke, R. A., O'Brien, P. J. & Carswell, D. A. (2000). Garnet zoning and the identification of equilibrium mineral compositions in high-pressure–temperature granulites from the Moldanubian Zone, Austria. *Journal of Metamorphic Geology* **18**, 551–569.

Ellis, D. J. (1987). Origin and evolution of granulites in normal and thickened crust. *Geology* **15**, 167–170.

Erambert, M. & Austrheim, H. (1993). The effect of fluid and deformation on zoning and inclusion patterns in poly-metamorphic garnets. *Contributions to Mineralogy and Petrology* **115**, 204–214.

Fernández-Suárez, J., Corfu, F., Arenas, R., Marcos, A., Martínez Catalán, F., Díaz García, F., Abati, J. & Fernández, J. (2002). U–Pb evidence for a polyorogenic evolution of the HP–HT units of the NW Iberian Massif. *Contributions to Mineralogy and Petrology* **143**, 236–253.

Fuhrman, M. L. & Lindsley, D. H. (1988). Ternary-feldspar modeling and thermometry. *American Mineralogist* **73**, 201–215.

González Cuadra, P., Martínez Catalán, J. R., Arenas, R., Díaz García, F., Abati, J. & Dunning, G. (1999). Polyorogenic evolution of the uppermost unit of the Órdenes Complex (NW Spain). *Journal of Conference Abstracts (EUG 10)* **4**, 34.

Hand, M., Scrimgeour, I., Powell, R., Stuwe, K. & Wilson, C. J. L. (1994). Metapelitic granulite from Jetty Peninsula, East Antarctica: formation during a single event or by polymetamorphism? *Journal of Metamorphic Geology* **12**, 557–573.

Harley, S. L. (1989). The origins of granulites, a metamorphic perspective. *Geological Magazine* **126**, 215–247.

Hiroi, Y., Kishi, S., Nohara, T., Sato, K. & Goto, J. (1998). Cretaceous high-temperature rapid loading and unloading in the Abukuma metamorphic terrane, Japan. *Journal of Metamorphic Geology* **16**, 67–81.

Indares, A. (1995). Metamorphic interpretation of high-pressure–temperature metapelites with preserved growth zoning in garnet, eastern Grenville province, Canadian shield. *Journal of Metamorphic Geology* **13**, 475–485.

Lieberman, J. & Petrakakis, K. (1991). TWEEQU thermobarometry: analysis of uncertainties and applications to granulites from western Alaska and Austria. *Canadian Mineralogist* **29**, 857–887.

Martínez Catalán, J. R., Arenas, R., Díaz García, F. & Abati, J. (1997). Variscan accretionary complex of northwest Iberia: terrane correlation and succession of tectonothermal events. *Geology* **27**, 1103–1106.

Martínez Catalán, J. R., Arenas, R., Díaz García, F. & Abati, J. (1999). Allochthonous units in the Variscan Belt of NW Iberia. In: Sinha, A. K. (ed.) *Basement Tectonics, 13*. Dordrecht: Kluwer Academic, pp. 65–84.

Newton, R. C. (1983). Geobarometry of high-grade metamorphic rocks. *American Journal of Science* **283-A**, 1–28.

Platt, J. P. (1986). Dynamics of orogenic wedges and the uplift of high-pressure metamorphic rocks. *Geological Society of America Bulletin* **97**, 1037–1053.

Powell, R. & Downes, J. (1990). Garnet porphyroblast-bearing leucosomes in metapelites: mechanisms, phase diagrams and an example from Broken Hill, Australia. In: Ashword, J. R. & Brown, M. (eds) *High-temperature Metamorphism and Crustal Anatexis*. London: Unwin Hyman, pp. 105–123.

Shiki, T. & Misawa, Y. (1982). Forearc geological structure of the Japanese Islands. In: Leggett, J. K. (ed.) *Trench–Forearc Geology; Sedimentation and Tectonics of Modern and Ancient Active Plate Margins*. *Geological Society, London, Special Publications* **10**, 63–73.

Spear, F. S. (1993). Metamorphic phase equilibria and pressure–temperature–time paths. *Mineralogical Society of America Monograph*, 799 pp.

Spear, F. S. & Florence, F. P. (1992). Thermobarometry in granulites. Pitfalls and new approaches. *Journal of Precambrian Research* **55**, 209–241.

Spear, F. S., Kohn, M. J. & Cheney, J. T. (1999). *P–T* paths from anatectic pelites. *Contributions to Mineralogy and Petrology* **134**, 17–32.

Thompson, A. B. & Connolly, J. A. D. (1995). Melting of the continental crust: some thermal and petrological constraints on anatexis on continental collision zones and other tectonic settings. *Journal of Geophysical Research* **100**, 15565–15579.

Tracy, R. J. (1982). Compositional zoning and inclusions in metamorphic minerals. *Reviews in Mineralogy* **10**, 355–397.

Tuccillo, M. E., Essene, E. J. & van der Pluijm, B. A. (1990). Growth and retrograde zoning in garnets from high grade metapelites: implications for pressure–temperature paths. *Geology* **18**, 839–842.

Warnaars, F.W. (1967). Petrology of a peridotite-amphibolite and gabbro-bearing polyorogenic terrain NW of Santiago de Compostela (Spain). Ph.D. thesis, University of Leiden, Netherlands, 208 pp.